Journal of Energy Storage 158 (2026) 121746

Contents lists available at ScienceDirect

Journal of Energy Storage

journal homepage: www.elsevier.com/locate/est

Research Papers

A bilevel model to optimize shore-to-ship connection systems with energy storage

Hugo Daniel [a], Loïc Boulon [b], João Pedro F. Trovão [a,c,d,*], David Williams [e]

[a] e-TESC Lab., University of Sherbrooke, Sherbrooke, QC, J1K 2R1, Qc, Canada
[b] Hydrogen Research Institute, University of Quebec at Three-Rivers, Qc, Canada
[c] INESC Coimbra, Department of Electrical and Computer Engineering, University of Coimbra, Polo II, 3030-290 Coimbra, Portugal
[d] Polytechnic of Coimbra, IPC-ISEC, DEE, 3030-199, Coimbra, Portugal
[e] Fednav Limited, Montreal, QC, H3B 4W5, Qc, Canada

ARTICLE INFO

Keywords:
Shore power
Bilevel
Optimization
Battery energy storage (BESS)
Port electrification
Mobile hydrogen generator
Marine microgrid

ABSTRACT

In the context of the maritime energy transition, this study addresses energy storage and electrical generation applications for shore power in green ports, combining the shore electrical distribution network, battery energy storage and a novel mobile hydrogen generation concept. An original bilevel optimization model is proposed, aiming to minimize port investment while optimizing the business model for the operation of the storage system. The model performs the sizing and planning-level power dispatch of the different energy sources and port configurations while ensuring optimal operating costs under the demand-charge electricity tariff. A test case on a dry bulk port with five berths resulted in an optimal configuration of a 891 kW budgeted power substation, a 367 kWh battery energy storage system, and one mobile hydrogen generator with a multi-stack fuel cell of 400 kW complemented by a battery with a capacity of 460 kWh. In the end, the proposed energy storage and mobile hydrogen generation solutions for shore power were able to reduce the levelized cost of electricity and the required peak power demand. Despite achieving a 63% cost reduction compared to reference scenarios, the optimal solution's annual profit remains negative at -$170 k, indicating a need for external financial support policies.

1. Introduction

As the global maritime industry undertakes the energy transition toward decarbonization, the deployment of shore-to-ship connections emerges as a fundamental solution. Shore-to-ship connections, also known as onshore power supply, alternative marine power, and cold ironing, are referred to as shore power in this text for clarity. Shore power is a decarbonization measure and technology that enables ships to shut down their diesel engines while in ports. An electrical connection supplies ships with green electricity from the shore, enabling the reduction of emissions by ~3 t to 150 t of carbon dioxide (CO_2) per day and per ship at berth, depending on the ship type and size [1]. Shore power is a fundamental decarbonization measure because it allows for an immediate reduction of greenhouse gas (GHG) emissions, it is more efficient than systemically using green fuels generated by electricity, and it can reduce air pollutant emissions affecting the health of the populations near ports. It is also enabling ships to access electricity, slowly preparing the world's ports and the international fleet of ships to transition toward microgrid solutions.

1.1. Problem description

Despite its significant advantages, shore power also encompasses major barriers discussed by Kim et al. [2] and Daniel et al. [3], such as: the large capital expenditure (CAPEX) required for the shore infrastructures, the different electricity pricing tariffs in the world and operational expenditure (OPEX), power availability, and the number of stakeholders involved. To mitigate the economic and power availability barriers, port-level solutions such as energy storage and distributed hydrogen generation could play an important role in reducing the size of the shore infrastructures and peak power requirements. Indeed, the ships connected to shore power require high-rated power capacity to supply peak demands, inducing high investments in electrical equipment. Also, the electrification of various industrial sectors is putting

* Corresponding author at: e-TESC Lab., University of Sherbrooke, Sherbrooke, QC, J1K 2R1, Canada.
E-mail address: joao.trovao@usherbrooke.ca (J.P.F. Trovão).

https://doi.org/10.1016/j.est.2026.121746
Received 27 June 2025; Received in revised form 17 March 2026; Accepted 21 March 2026
Available online 26 March 2026

significant pressure on the electrical grid, sometimes resulting in limited power delivery. Finally, the shore power infrastructures do not have a good utilization rate compared to conventional electrical installations, as there is not always a ship at berth to use the system.

Therefore, solutions such as battery energy storage systems (BESS) and mobile hydrogen generators could reduce the total cost of shore power systems and related operational costs. Following the fundamental synthesis work on green port and port energy-storage research from Iris and Lam [4], BESS is treated as a central mitigation option because batteries enable peak shaving, load shifting, renewable integration and grid-service provision that can substantially reduce the need for costly substation upgrades and lower lifecycle operating costs. Additionally, Semchukova et al. [5] have shown that modular hydrogen generation provides modularity and geographic flexibility that can overcome the grid-capacity and location-specific constraints of remote or low-utilization berths, avoiding high CAPEX for substation extensions. The authors also mention that fuel cell systems for shore power applications can be deployed onshore or on barges for shore power.

Conversely, the optimal investment cost in port-level shore power deployment systems does not automatically result in optimal profits because the long-term operating cost is dependent on the initial design (capacity of the shore power substation, BESS, and hydrogen generator). Therefore, two entities are competing against each other in the port shore power deployment problem: the port investors and the shore power operators. A bilevel model formulation problem is required to address this problem because the investment (CAPEX) decisions made by the investor (leader or upper problem) inherently determine the feasible operating strategies, parameters, and economic configuration available to the operators of the shore power system (follower or lower problem). Based on Sinha et al. [6], bilevel models are “mathematical programs where an optimization problem contains another optimization problem as a constraint”, and are specifically suited to hierarchical problems in which an upper-level entity commits to infrastructure, capacity limits or tariff settings and a lower-level entity then optimally dispatches resources and chooses operational strategies to minimize OPEX or maximize profit.

Fig. 1 presents such a problem space with: the upper level space (the investors), the lower level space (the operators), the feasible solutions constrained by the upper level parameters, the exchange of parameters from the upper level to the lower level, and the parametric optimization space of the lower level.

In this context, the investor (leader) chooses component sizing and the electrical distribution layout. Then, the operator (follower) reacts by fixing BESS charging/discharging strategies, procuring grid power or dispatching distributed generation mobile units.

Real-world port decision-making is hierarchical and split across stakeholders: port authorities, terminal operators, local governments and utilities. For example, Innes et al. [7], the Aberdeen shore power case, is a strong real-world study that helped democratize shore power but focuses on investor-side CAPEX and models electricity with a fixed price, without including the demand-charges of power, time-of-use tariffs, or an operational dispatch. Because operational responses (dispatch, procurement and pricing) materially affect lifecycle OPEX and capacity needs, a bilevel leader–follower framework is necessary to capture the strategic coupling between investment and operation of shore power. A single-level centralized model assumes perfect coordination, which is rarely achievable in practice.

The following section reviews the literature on marine port energy storage and distributed generation optimization, and how these optimization issues are handled in other works. The literature review is concluded with a summary of the research gaps and is followed by a section detailing the contributions, i.e., how this work addresses the research gaps.

1.2. Literature review

In the context of marine green ports with shore power applications, a key dimension revolves around attaining optimal component sizing to meet specific power demands and facilitate efficient microgrid planning. Gutierrez-Romero et al. [8] conducted a comprehensive investigation into ship calls at the port of Cartagena, Spain, to assess the power requirements of berthed ships. They analyzed the availability of wind and solar resources and determined that renewables should be integrated into marine port microgrids to cover the shore power demand and perform the microgrid planning. Caprara et al. [9] explored strategies to reduce the required maximum power demand of shore power in cruise ports. Their approach involved using the batteries for load shifting, storing excess renewable energy, and coordinating with diesel generators. The component sizing is done with in-house software and an iterative approach, and showed that a battery can prevent the construction of additional power substations to cover shore power needs. Their main finding is that a compromise between the BESS and the shore power connection system's maximum power helps to reduce the total cost.

Efficient energy management lies at the core of marine port microgrid operations, and a crucial aspect involves optimizing the power dispatch process through advanced algorithms. Iris & Lam [10] addressed uncertainty in renewable energy and smart grid integration. Their energy management method is based on a mixed integer programming model and solved with the CPLEX 12.7 solver. The paper demonstrated that microgrids are a better option than conventional systems to address different loads in ports. Additionally, Tang et al. [11] implemented model predictive control to optimize power dispatch in a maritime hybrid energy system. This study emphasizes minimizing electricity costs during ship berth periods, illustrating the importance of advanced control algorithms in achieving cost-effective energy management. Xia et al. [12] optimized energy management using genetic

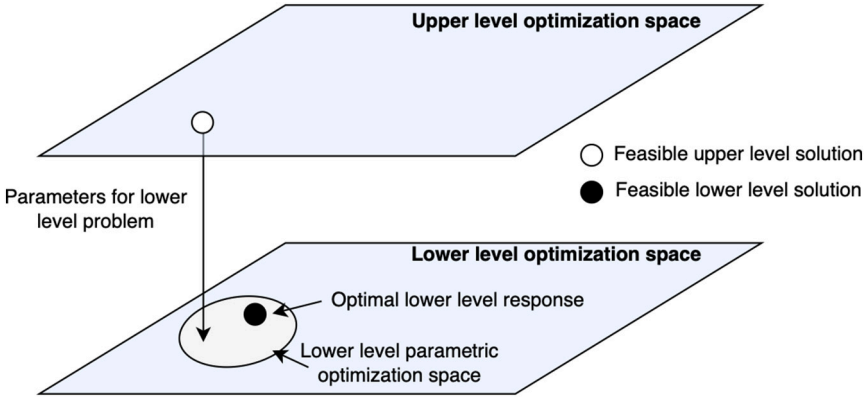

Fig. 1. Bilevel general architecture (inspired from Sinha et al. [6]).

algorithms (GA) and particle swarm optimization, aiming to lower power supply costs by effectively coordinating wind, solar, and grid sources. This showcases the role of heuristic algorithms in achieving less expensive energy management costs than traditional power costs. Subsequently, Song et al. (2022) [13] focus on energy management in ports using the alternating direction method of the multipliers algorithm. Their takeaway is that carbon capture and carbon trading can play an important role in the decarbonization of ports, but it should relate to renewables and the grid to ensure reliability. Conte et al. [14] introduce a model predictive control energy management approach for a port featuring shore power connections and hydrogen supply for ships. Their energy storage and distributed generation design includes renewable energy, hydrogen electrolysis, storage, batteries, and the grid, with stochastic optimization accounting for renewable resource uncertainty and was able to accurately respond to the energy demand of the ships. Lastly, Wang et al. [15] proposed an energy management model for ports regarding ships in port as a group of many users with renewable energy generation equipment or energy storage equipment. The authors call this group of users the "we-energy" group. Their approach aims to minimize costs by effectively integrating wind, solar, grid, energy storage, and traditional plant sources. The problem is solved with a consensus algorithm. The results showed the relevance of we-energy in diminishing cost.

Within marine green port studies, the adoption of multi-agent systems offered concluding results to elevate power management and resource allocation strategies. Zhang et al. [16] employed distributed optimization algorithms and multi-agent systems in the energy management of seaports with energy storage and distributed generation systems. Their focus on cost minimization through optimized utilization of wind, solar, grid, heat, gas, and energy storage underscores the importance of collaborative algorithms to optimize energy management and effectiveness for large ports. Also, Kanellos et al. [17] proposed an innovative power management method for ports based on a multi-agent system. However, when compared to the centralized method, the results of the operating costs were very similar while requiring larger computational time.

In the pursuit of comprehensive marine green port optimization, a notable approach involves the simultaneous integration of sizing and energy management models. Ahamad et al. [18] propose a model to find the optimal sizing of future marine port energy storage and distributed generation systems to supply shipboard load. In [19], Molavi et al. propose a two-stage stochastic programming approach to determine how some "Smart Port Index" metrics can be integrated into the microgrid planning of ports and augment the smartness of ports. The first stage consists of an investment problem, and the second stage is a multi-objective operation planning subproblem: power dispatch, load shedding and power flow between the microgrid and the grid. The model is solved with Benders decomposition and Lexicographic Goal Programming is applied to the subproblems. The results proved that the proposed model could guarantee improvements in productivity, sustainability, environment and reliability of operations. Lastly, in [20], Wang et al. propose a two-stage model that is capable of determining the optimal capacity of components for renewable energy systems in marine ports. To optimize the solution, the authors use an iterative approach that selects different setting parameters in the first stage and the second stage determines if they are feasible based on stochastic optimization of renewable resources and power dispatch.

An advantage of multiple-stage methods is that they enable finding a trade-off between the sizing of the components and power dispatch for minimum costs. To optimize the search for optimal solutions, bilevel models are utilized in classic land microgrid planning. As a result, Haghifam et al. [21] proposed a bilevel model for optimal land microgrid sizing and operation. While not focused on marine green ports, this model balances investment and operational costs while optimizing system design, showcasing the importance of bilevel algorithms in finding the optimal configuration of the energy storage and distributed generation components, considering the constraints of energy management. To solve the model, it is transformed into a linear single-level model with the use of Karush–Kuhn–Tucker conditions. Alternatively in [22], a bilevel model is used to perform the optimal design for a hybrid ferry by simultaneously optimizing the components sizing and the optimal energy management for a typical route of a ferry. The model was successful in optimizing both component sizing and an optimal power dispatch with a sine cosine algorithm improved with harmony search.

As suggested by Sinha et al. [6] in their review of bilevel models, evolutionary computation such as GA have a lot of practical applications in the field of optimization. Bilevel optimization is, based on the authors' definition, "a mathematical program, where an optimization problem contains another optimization problem as a constraint." They also show that bilevel research is actively increasing in the fields of electric power, supply chain and policies. For example, Hajiaghaei-Keshteli and Fathollahi-Fard [23] have developed a two-stage stochastic bilevel decision-making model for distribution network problems, which shows better computational performance than other traditional models. Haghifam et al. work [21] also discusses bilevel models for microgrid design and planning, but it is not adapted to marine green ports supplying shore power. João Alves et al. [24] developed a new bilevel model for setting electricity time-of-use tariffs where both the periods and the prices are decision variables, which could be relevant for shore power. The new model includes a GA in the upper optimization problem and a mixed integer linear programming problem in the lower level showing improved performance.

In conclusion, the literature has addressed the optimal energy management and sizing of renewable energy systems for marine port energy storage and distributed generation. It was found that it is feasible to reduce costs. However, the literature review also showed that there is a research gap regarding the two optimization problems of marine green ports for shore power: the shore power investor and the shore power operator problems. A new bilevel model adapted to marine green ports supplying shore power to find the best trade-off between component sizing and power dispatch would be needed as these models have shown great results in conventional land-based networks. Also, most of the studies considered in the review are using renewables to store energy that can be sold back to the grid in periods of low power demand. However, this solution does not solve the issue of high CAPEX for remote berths with low utilization rates like a mobile generating unit could. Only one article mentions the use of BESS to limit the power demand on the grid, which could improve the OPEX of shore power systems. Finally, the mobile hydrogen generator with a hybrid battery-multi-stack fuel cell system has never been studied, and it could be a solution for shore power at remote berths or berths with low utilization rates.

1.3. Contributions

Based on the problem description and the literature gaps, a bilevel model is proposed to solve the optimization problem including the shore power system designer represented by the port investors entity, and the shore power system operator represented by the terminal operator entity. The goal of the proposed bilevel model is to reduce the CAPEX of the port and the OPEX of the terminal operator by reducing the total annual cost of shore power and limiting the power demand of shore power on the local grid, which optimizes overall profits. To evaluate the model, a test case is performed on a typical bulk terminal.

The article makes the following significant contributions:

- Introduces an innovative bilevel model adapted for marine port energy storage and distributed generation systems incorporating shore power design, optimization of component sizing, placement of shore power connections, and energy management while accounting for limited grid power availability.

- Investigates the use of Battery Energy Storage Systems (BESS) and mobile hydrogen generators to overcome the economic and power constraints associated with shore power.
- Proposes mobile hydrogen generators as a viable alternative to grid-based shore power connections for berths with low utilization rates, enhancing flexibility and reducing costs.
- Provides a novel technical-economic analysis of shore power solutions with energy storage and distributed generation systems, specifically in bulk terminals, offering fresh insights into their potential efficiency and sustainability.

These advancements establish a new framework for improving the energy management of marine ports, promoting a more sustainable future in maritime operations. The rest of the document is organized as follows: Section 2 details the methodology, Section 3 presents and discusses the results of the test case, and Section 4 concludes with the important findings.

2. Methodology

According to Fig. 2, the high-level structure of the proposed port bilevel shore power deployment problem is defined with the entity making the CAPEX investment at the upper level, and the entity operating the shore power system at the lower level. Then, the operators provide shore power services to the ships at a defined rate. Hence, the lower optimization problem is nested in the leader optimization problem and uses the leader outputs as constraints.

The two optimization problems are competing against each other as the investors want a low investment shore power system, but the operators want a system that is not expensive to operate, and therefore more CAPEX intensive in some cases:

- Upper optimization problem (leader): Port investors
  - Goal: minimizing the capital investment, i.e., the CAPEX and annual profit
  - This problem represents the investor's and funding entity's perspective.
  - The variables that are optimized are the size of the different energy source and storage components, and the shore power distribution network design.
- Lower optimization problem (follower): Terminal operator or shore power system operators
  - Goal: minimizing the operational cost.
  - This problem represents the shore power facility operators' perspective.
  - The variables that are optimized are the values of power supplied by each energy source and storage components, i.e., the power dispatch.

As different energy sources and energy storage system sizing will result in different feasible operating schemes, the two entities (upper and lower problem) need to negotiate parameters to find the optimal solution.

The port's shore power energy source and energy storage dispositions and interactions are presented in Fig. 3. The dotted line arrows represent the flow of information, control commands, and decision-making between each system, while the solid line arrows represent the power flows. The grid and hydrogen are the two energy sources considered, while the BESS and the hydrogen generator battery are the two energy accumulators. The power flows from the sources to the load, which are the ships or the batteries when recharged as described by the arrows.

First, the shore power designers (port investors) take the information from the ship berth visits, power demand, peak demand, etc. and make an initial decision over design and sizing of the energy sources. They also identify the distribution layout, which includes the berths to electrify with a shore power connection and the berths to supply with the mobile hydrogen generator, with the aim of covering 100% of the berths with shore power service and to have a zero-emission port. The berth utilization, the visiting ship types, the location, etc., of each berth will highly impact the energy source sizing, energy storage design process, and resulting optimal solution. Then, the operators determine the optimal power dispatch from the different energy sources and supply the ship's power demand accordingly.

The power flows are represented in Fig. 3 where P^{Grid} is the power from the grid, P^{Subst} is the power from the electrical substation, P^{BESS} is the power from the BESS, P^{FC} is the power from the hydrogen generator multi-stack fuel cell, P^{BHGen} is the power from hydrogen generator's battery, P^{HGen} is the total power from the hydrogen generator, and P^{SP} is the power demand from the ships using shore power.

The following sections detail the different aspects of the model such as the energy sources, the electrical distribution network layout, the shore power system investor optimization problem, the shore power system operator optimization problem, and the bilevel problem formulation.

2.1. Energy sources

In the energy source sections, the BESS, the utility grid and the mobile hydrogen generator models are detailed.

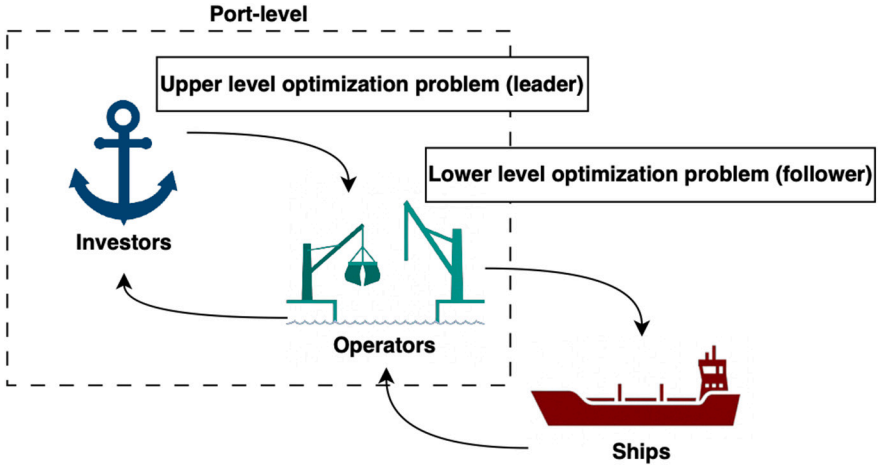

Fig. 2. High-level structure of the bilevel problem.

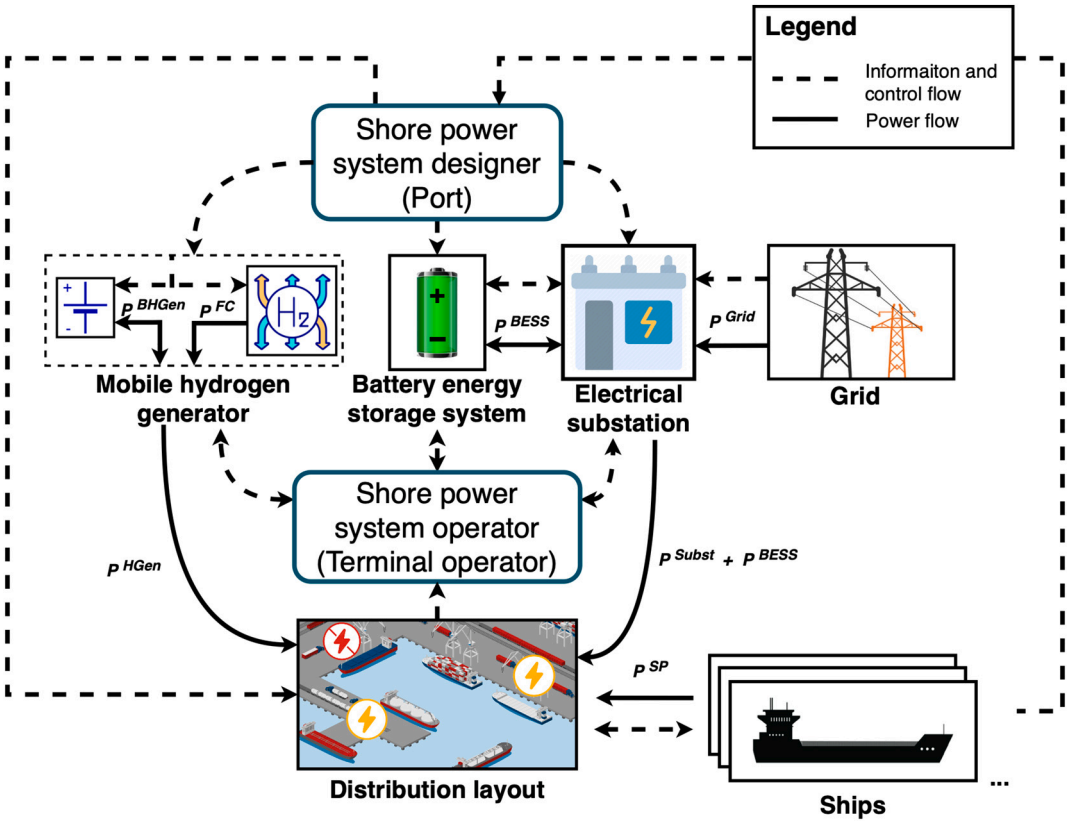

Fig. 3. Marine port shore power energy source and energy storage system landscape and interactions.

2.1.1. Substation and utility grid

An electrical substation is required in any shore power project. This infrastructure integrates electronic controls, and the main transformer converts the voltage from the grid to the voltage transferred to the ships. Eq. (1) describes the substation:

$$P_{(t)}^{Subst} \leq P_{max}^{Subst} \tag{1}$$

where t is the time unit with $t \in T$, T is the set of hours in a day: $T = \{t_1, t_2, \ldots, t_{24}\}$.

The grid is the main supplier of energy. While renewables could also supply the port with clean energy, the integration of the renewables would be done at a higher level and fed into the shore power electrical network. It is considered that the transmission lines connecting the electrical substation of the port to the main substation of the electrical provider are high voltage, i.e. 25 kV or other, and that the power required by ships at berth is much smaller than the total capacity. For this reason and to simplify the model, the grid can be seen as an infinite source of power and energy. The following Eq. (2) determines the hourly power supplied by the grid:

$$P_{(t)}^{Grid} = P_{(t)}^{Subst} \tag{2}$$

2.1.2. Battery energy storage system

The BESS is a critical component to store energy and performing peak shaving. Also, thanks to the fast dynamic nature of batteries [25], it is considered that the BESS smoothens the power demand and eliminates the fast transient peak power demands. The BESS is connected directly to the port electrical distribution network and is controlled automatically. The following equations present the model for the BESS:

$$P_{(t)}^{BESS} = P_{(t)}^{Bat} \times \eta_{eff}^{Bat} \tag{3}$$

$$SOC_{(t)} = SOC_{(t-1)} + P_{(t)}^{BESS} \tag{4}$$

$$SOC_{min} \leq SOC_{(t)} \leq SOC_{max} \tag{5}$$

$$SOC_{max} = 0.95 \times Q^{BESS} \tag{6}$$

$$SOC_{min} = 0.2 \times Q^{BESS} \tag{7}$$

$$P_{(t)}^{BESS} \leq P_{max}^{BESS} \tag{8}$$

$$SOC_{t_0} = SOC_{t_{24}} = SOC_{max} \tag{9}$$

where P^{Bat} is the power of the battery before applying the efficiency losses, η_{eff}^{Bat} is the electrical efficiency factor of the battery, SOC is the state-of-charge (SOC) of the battery, Q^{BESS} is the energy capacity of the BESS, and P_{max}^{BESS} is the maximum power of the BESS system.

The average power should not exceed 0.5C of the battery's nominal capacity (P_{max}^{BESS}), which is a conservative value for typical LFP microgrid cells [26]. Then, the efficiency factor is set to 98%. Also, to prevent premature battery aging, the SOC of the battery is set to vary between 95% and 20%. As detailed by B. Xu et al. [27] Lithium-ion battery technologies can withstand about 5000 equivalent cycles (N_{Cycles}) before losing about 20% capacity. After this period, the battery needs to be replaced. The number of equivalent full discharge cycles as defined in (10) and is based on the total cumulated energy supplied by the battery, excluding the energy used to recharge the battery:

$$N_{Cycles} = \frac{\sum_{t_c=1}^{N_{Tc}} P_{(t_c)}^{BESS} \times \Delta t(t_c)}{Q^{BESS}}, with\ t \in T_C\ if\ P_{(t)}^{BESS} > 0 \tag{10}$$

where T_C is a subset of time t where the battery supplies power to the grid with $t_c \in T_C = \{t_{c(1)}, t_{c(2)}, \ldots t_{c(N_{Tc})}\}$, and N_{Tc} is the total number of time data point in T_C.

However, more detailed battery degradation models can estimate the

state of health using multiple criteria, including electrochemical models, equivalent circuit-based models, performance-based models, analytical models with empirical fitting, and statistical approaches [28].

2.1.3. Mobile hydrogen generators

Multi-stack fuel cell systems have recently gained more traction for high-power system applications [29]. The mobile hydrogen generator uses a multi-stack fuel cell system to produce green electricity and is used as an alternative energy source to the grid as it can be displaced to different locations. This alternative is cost-effective compared to traditional grids in case of extremely low utilization rate of the berths by the ships, which results in prohibitive electrification costs. As multiple containerized solutions exist for the hydrogen generator and the hydrogen tank, the challenge is to determine the right sizing for specific shore power applications. It is also considered that the tank is refilled with green hydrogen from a local distribution center when the system is not used, and that the tank of the mobile system can be large enough to accommodate a ship during its entire stay in port. The assumptions about the containerized system, the hydrogen tanks, and the transportation of the hydrogen are based on the works of the US Department of Energy [30] [31].

Furthermore, the hydrogen generator is designed with a battery to prevent the multi-stack fuel cell system from being used in inefficient modes and to compensate for the abrupt variations in power, which can damage the multi-stack fuel cell system. Therefore, a factor β of 90% is applied to distribute the energy supplied by the hydrogen generator between the multi-stack fuel cell system and the battery. It means that the battery is constantly supplying 10% of the energy except when it is being recharged. The following equations present the model of the hydrogen generator:

$$mH_{(t)} = P^{FC}_{(t)} \Big/ \eta^{FC}_{eff} \bullet \frac{3.6MJ/kWh}{119.96MJ/kg} \tag{11}$$

$$P^{HGen}_{(t)} = P^{FC}_{(t)} + P^{BHGen}_{(t)} \tag{12}$$

$$P^{FC}_{max} = N^{s} \times P^{mFC}_{max} \tag{13}$$

$$P^{FC}_{min} \leq P^{FC}_{(t)} \leq P^{FC}_{max} \tag{14}$$

$$P_{FC(t,f)} = \begin{cases} \beta \times P^{SP}_{(t,b_f)}, & SOC^{BHGen} > SOC_{min} \\ P^{SP}_{(t,b_f)} + P^{BHGen}_{(t)}, & SOC^{BHGen} \leq SOC_{min} \end{cases} \tag{15}$$

where mH is the mass of hydrogen consumed by the fuel cells for the hydrogen generator f with $f \in F$, F is the set of mobile hydrogen generators, η^{FC}_{eff} is a factor representing the efficiency of the multi-stack fuel cell system, N^{s} is the number of fuel cell stacks, and P^{mFC} is the power of a single stack of fuel cells.

Real fuel cells efficiency (η^{FC}_{eff}) is following anon-linear relation. However, it is common to use constant approximations for planning-stage-level analysis. Further precise models can be integrated into the model if required. Also, this work uses a basic fuel cell degradation model assuming a useful lifetime of 10,000 h based on [32]. Nevertheless, more detailed degradation models that explicitly account for start-stop operation, idling, load changes, and high-power operation can also be implemented to improve degradation accuracy [33].

The battery of the hydrogen generator uses the same model as the BESS in Section 2.1.2, but with its own sizing of the battery capacity Q^{BHGen}, and its own state of charge SOC^{BHGen}.

2.2. Berth layout for the port electrical distribution network

The berth layout divides the berths of the studied set of berths in a marine terminal into two categories: the berths to connect to the port electrical distribution network and the berths to service with mobile hydrogen generators. All combinations of berths are investigated by the model. The distance between each berth and the berth utilization will have an important impact on the results because of the underground cables' installation cost.

The mobile hydrogen generator can reduce the costs of shore power infrastructures because one system can cover multiple berths that are less utilized or remote. However, there must be a reasonable number of mobile hydrogen generators to cover the case where multiple ships are present at the same time at these berths.

To ensure the hydrogen generator can supply the ships in such an event, the proposed algorithm uses a statistical threshold, λ_{Tresh}, and the measured probability of having fewer mobile hydrogen generators than ships at berth, $\lambda_{Multiple\ ship}$, to determine the quantity of mobile hydrogen generators N^{HGen} to have. The algorithm flowchart is presented in Fig. 4.

The probability of having more ships than hydrogen generators takes into consideration that a risk of zero is oversized. Therefore, the statistical threshold, λ_{Tresh}, is set to allow one occurrence every 3 years and can be modified based on the designer requirements. $\lambda_{multiple\ ship}$ equation is presented in (16):

$$\lambda_{multiple\ ship} = 1 - \prod_{b=1}^{\Lambda} (1 - \lambda_b) \tag{16}$$

where λ is the probability of having a ship at a berth i to be occupied by a ship, and Λ is the set of probabilities λ_b for the berths that will be supplied by a hydrogen generator with $\Lambda = \{\lambda_1, \lambda_2, \ldots \lambda_\Lambda\}$.

The model assumes that ships call specific remote berths because those berths are required for particular cargo operations: unique handling equipment, permitted draft, or contractual concession rights. Such calls are generally not reallocated without substantial operational or commercial consequences. Reallocation would typically impose routing delays, extra port fees and cargo-handling costs expected to exceed any marginal savings from using a different electrified berth. Relocating calls is known in the literature as a berth-and quay-crane allocation problem [34]. It is common in container and dry-bulk terminal shore power studies, but these consider cases where not all berths are electrified.

2.3. Optimization framework

The proposed optimization framework is a bilevel model, presented in Fig. 5, that jointly optimizes investment and operation for port-level shore power systems in zero-emission ports. The model takes as inputs annual berth power-demand profiles, utilization forecast and component cost data provided by the port, and it returns CAPEX, OPEX, energy consumption, the electrical-distribution layout and component sizing as outputs.

At the upper level (the shore power system designer, represented by the port investors), the decision variables include the BESS capacity, the substation maximum budgeted power, the mobile hydrogen-generator sizing, the hydrogen-generator battery capacity, and the port layout (which berths are electrified). These upper-level choices define capacity limits and technical constraints that the lower level must respect.

The lower level represents the shore power system operator (the terminal operator) and solves the time-resolved power-dispatch problem: charging/discharging the BESS, power from the substation, and operating and dispatching the mobile hydrogen generators to minimize operating cost subject to the upper-level parameters.

The lower-level solver uses a dual-simplex linear algorithm to compute hourly dispatch and resulting operating costs. Because the lower-level feasibility and OPEX depend on the infrastructure set by the leader, the lower-level outputs (feasibility, dispatch schedules and OPEX) feed back to the upper level and influence the leader's search as a constraint. Therefore, the upper level uses a genetic algorithm to explore candidate infrastructure configurations, and each candidate is evaluated

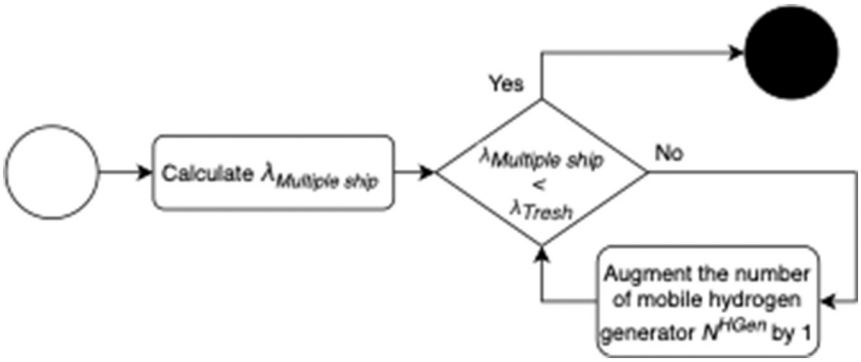

Fig. 4. Flowchart of the algorithm determining the number of hydrogen generators to use.

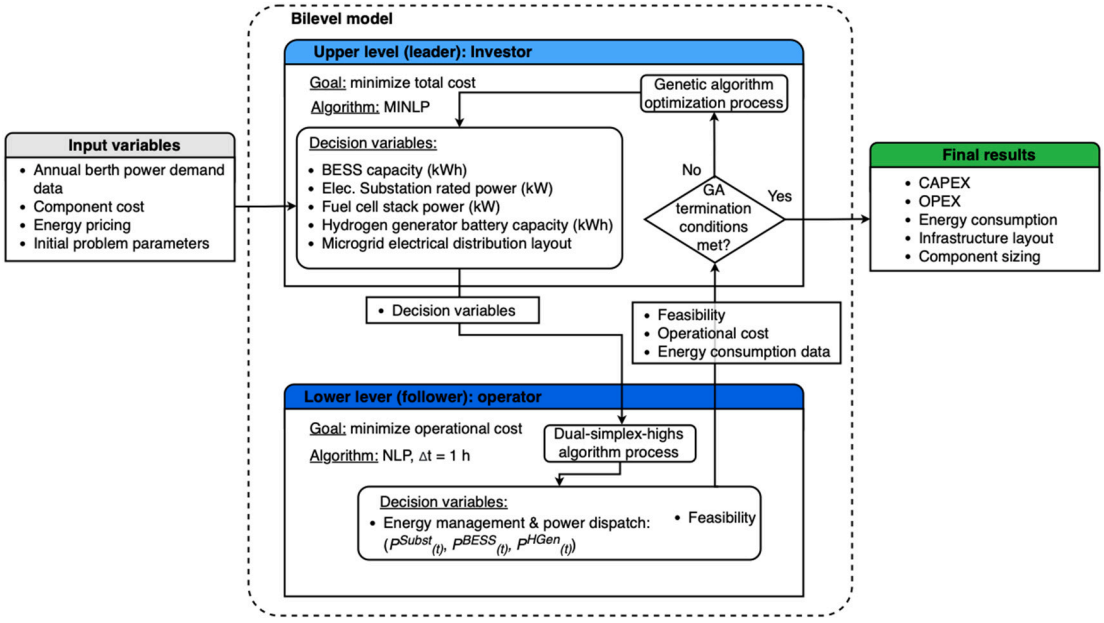

Fig. 5. Bilevel model algorithm architecture with decision variables, inputs and outputs.

by the lower-level optimization. Infeasible or costly operational responses penalize the candidate in the GA fitness function. In this way, the designer (investors) and the operators are effectively negotiating sizing and operation: the bilevel formulation finds solutions that minimize total lifecycle cost rather than CAPEX or OPEX alone.

The following section further details each element of Fig. 5.

2.3.1. Leader: shore power system designer problem (investors)

The objective of the shore power system designer upper problem is to minimize the investment. Because a low CAPEX will not result in an optimal investment, the objective of the shore power system designer is converted to maximize the annualized profits $Profit_a$ as defined in (17). The input variables of the upper problem are: the electrical substation maximum budgeted power P^{Subst}_{max}, the BESS capacity Q^{BESS}, the number of stacks in the multi-stack fuel cell system N_S, the hydrogen generator battery capacity Q^{BHGen}, and the electrical distribution layout: l. These variables are generated by the GA to find optimality and sent to the lower level for the parametric optimization process of the second layer.

$$Profit_a = \max_{P^{Subst}_{max},\ Q^{BESS},N^S,Q^{BHGen},\ l} \left(I^{Tot}_a - C^{Tot}_a\right) \tag{17}$$

with:

$$C^{Tot}_a = C^{Subst}_a + C^{BESS}_a + C^{HGen}_a + C^{BHGen}_a + \sum_{m\in M}\left(C^{ElecGrid}_{(m)} + C^{PowerGrid}_{(m)} + C^{H}_{(m)}\right) \tag{18}$$

$$I^{Tot}_a = \sum_{m\in M}\left(I^{ElecSP}_{(m)} + I^{ConnSP}_{(m)}\right) \tag{19}$$

where C^{Tot}_a is the total annual cost, C^{Subst}_a is the annualized CAPEX of the electrical substation, C^{BESS}_a is the annualized CAPEX of the BESS connected to the substation, C^{HGen}_a is the annualized CAPEX of the mobile hydrogen generators, C^{BHGen}_a is the annualized CAPEX of the mobile hydrogen generators' batteries, $C^{ElecGrid}$ is the cost of electricity for the substation, m *is* the month $m \in M$, M is the set of months of the year, $C^{PowerGrid}$ is the cost of power for the substation, C^{H} is the cost of hydrogen, I^{Tot}_a is the total annual income, I^{ElecSP} is the income of electricity sold to ships, I^{ConnSP} is the total income of from the ship connection fees to shore power, and l is an integer $l \in L = \{L_1, L_2, L_3, \ldots L_K\}$ representing the berth layout i.e. the arrangement identifier specifying the number of berths to electrify and the number of berths to supply with the mobile hydrogen generator.

The cost of electricity has two components, an energy component in [$/kWh] and a demand-charge component in [$/kW]. These variables can be adjusted depending on the port location and agreement with the

electricity provider to represent different tariff forms such as demand-charge, time-of-usage, day-ahead, or even fixed cost.

The generalized annualized cost (C_a) formula is presented in (20):

$$C_a = \left(C_I + \frac{C_R}{(1+i_r)^{n_r}}\right) \frac{C_I \times i_r}{1-(1+i_r)^{-n}} \tag{20}$$

where C_I is the total asset investment cost, C_R is the replacement cost which equals the asset investment cost, i_r is the interest rate, n_r is the time before an asset replacement, and n is the total recovery period of the project.

Based on Section 2.1, only the batteries and fuel cells are subject to replacement during the project period, which is proportional to their utilization. The total investment cost formulas are presented below:

$$C_I^{Subst} = z^{Subst} \times \left(P_{max}^{Subst} \times C^{Subst} \times CF + C_{base}^{Subst} + D_{(l)}^{Dist} \times C^{Dist} + N_{(l)}^{CMS} \times C^{CMS}\right) \tag{21}$$

$$C_I^{BESS} = z^{BESS} \times Q^{BESS} \times C^{Bat} \tag{22}$$

$$C_I^{FC} = z^{FC}\left(C^{Htruck} + N^{HGen} \times \left(P_{max}^{FC} \times C^{FC} + C^{Htank} \times C^{CMS}\right)\right) \tag{23}$$

$$C_I^{HGen\ Bat} = z^{BHGen} \times Q^{BHGen} \times C^{Bat} \tag{24}$$

where C_I^{Subst} is the total investment cost of the substation, z^{Subst}, z^{BESS}, z^{FC}, and z^{BHGen} are binary variables representing the use of the substation, the substation BESS, the multi-stack fuel cell system, and the hydrogen generator battery respectively. They equal 1 if the source is used and 0 if the system is not used. C^{Subst} is the cost of the substation, C_{base}^{Subst} is the base cost of the substation, CF is a 30% contingency factor for the maximum substation power, D^{Dist} is the function of the length of the distribution network, C^{Dist} is the cost of the distribution network, N^{CMS} is the number of cable management systems (CMS) to install, C^{CMS} the cost per cable management system, C_I^{BESS} is the total investment cost of the substation BESS, C^{Bat} is the battery cost, C_I^{FC} is the total investment cost of the hydrogen generator's multi-stack fuel cell system, $C_I^{HGen\ Bat}$ is the total investment cost of the hydrogen generator battery, C^{Htruck} is the cost of the truck carrying the hydrogen generator and its tank in a container, C^{Htank} is the cost of the hydrogen tank trailer, and C^{FC} is the cost of the fuel cells.

The cable management system is located on shore for bulk carriers, but for other ship types, the location will depend on the requirements of the shore power standard IEC/IEEE 80005–1. To allow mobile cable management systems and flexible designs, it is assumed that the number of cable management system to acquire, N^{CMS}, uses the same statistical analysis as the number of mobile hydrogen generators detailed in Section 2.1.3.

The operational cost of electricity, power, and shore power revenues are presented below:

$$C_{(m)}^{ElecGrid} = C_{(d,m)}^{Elec\ opt} \times \frac{Q_{(d,m)}^{Subst}}{Q_{(m)}^{Subst}} \tag{25}$$

$$C_{(m)}^{PowerGrid} = C_{(d,m)}^{Power\ opt} \tag{26}$$

$$C_{(m)}^{H} = C_{(d,m)}^{H\ opt} \times \frac{Q_{(d,m)}^{HGen}}{Q_{(m)}^{HGen}} \tag{27}$$

$$I_{(m)}^{ElecSP} = C^{ElecSP} \times Q_{(m)}^{SP} \tag{28}$$

$$I_{(m)}^{ConnSP} = I^{SPop} \times N_{(m)}^{conn} \tag{29}$$

where $C^{Elec\ opt}$ is the optimal electrical cost for the port, d is the day of the year for $d \in D$, D is the set of days of the year, Q^{Subst} is the total electrical demand of the substation to the grid, $C^{Power\ opt}$ is the optimal power cost, $C^{H\ opt}$ is the optimal hydrogen cost, Q^{HGen} is the energy demand for the mobile hydrogen generators, I^{SPop} is the port operational income per ship connections, N^{Conn} is the number of ship connection to shore power, Q^{SP} is the electrical energy demand of the ships using shore power, and C^{ElecSP} is the cost of electricity sold to the ships.

To obtain the monthly energy demand Q^{Subst}, the daily energy usage is used and multiplied by the number of days N^{Day} per month and with the ratio of berth b usage per month U:

$$Q_{(m)}^{Subst} = N_{(m)}^{Day} \sum_{b \in B^{Subst}} \sum_{t=1}^{T} U_{(b,m)} \times P_{(m,t)}^{Subst} \tag{30}$$

where B^{Subst} is the set of berths connected to the electrical distribution network, and T is the set of hours in the day.

Then, the monthly cost of power $C^{Power\ opt}$ is proportional to the peak power demand that occurred during the month. The typical monthly peak power demand varies with the time of the year and with the power demand of ships at berth.

The resulting monthly cost structure is used to reduce computing time, while keeping a good seasonal representativeness of berth usage and power demand variations. However, the model can be adapted to encapsulate more granular data or further forecast data.

Finally, the lower optimization problem might return infeasible solutions because the design parameters can lead to infeasible power dispatch, i.e., when the lower optimization algorithm is unable to satisfy its constraints with the given parameters as described in Section 2.3.2. In this case, a penalty factor is applied to the $Profit_a$ function in (31). This penalty function enables to the discarding of infeasible solutions by making them extremely expensive and indicating to the search algorithm to search other areas.

$$\begin{aligned} &if\ C_{(d,m)}^{Elec\ opt}\ not\ feasible,\ \ Profit_a = Profit_a + Penalty^{Factor} \\ &\qquad with\ Penalty^{Factor} \to -\infty \end{aligned} \tag{31}$$

Because the upper-level objective $Profit_a$ is maximized, infeasible lower-level solutions are discouraged by adding a large negative penalty to the objective. Formally, the penalty factor is required to tend toward negative infinity so that any infeasible solution has low fitness and is effectively eliminated by the GA. In the numerical experiments, the penalty was implemented as a large finite constant of -1×10^8.

The problem is dependent on nonlinear components such as the non-linear relation between the energy source and energy storage systems' capacity, and the resulting profit of the solution. The problem is also dependent on integer components such as the berth layout. Therefore, the resulting problem is non-linear mixed-integer programming (MINLP).

Several solution approaches were evaluated, and the GA was retained because the overall formulation is a mixed-integer nonlinear problem with a large, nonconvex search space driven by discrete berth-layout decisions. As a population-based meta-heuristic algorithm, GA provides robust exploration and can consistently identify high-quality feasible solutions within practical runtimes, whereas gradient-based nonlinear solvers may be sensitive to initialization and prone to convergence to local optima in this setting.

Fig. 6 presents the flowchart of the GA used to solve the leader problem. The GA was implemented using MATLAB's GA solver with an initial population matrix. The main parameters were set to a population size of 80, an elite count of 15, a maximum stalled generations of 120, a maximum number of generations of 250, and a fitness function tolerance of 1×10^{-3}.

In the beginning, the algorithm generates the initial population of substation maximum power, BESS size, multi-stack fuel cell maximum power, mobile hydrogen generator battery size and berth layout. Then it calculates the fitness function, i.e., the annualized profit based on the annualized investment cost of the components of Eq. (17), and the lower-level optimal operating costs. However, in the case where the

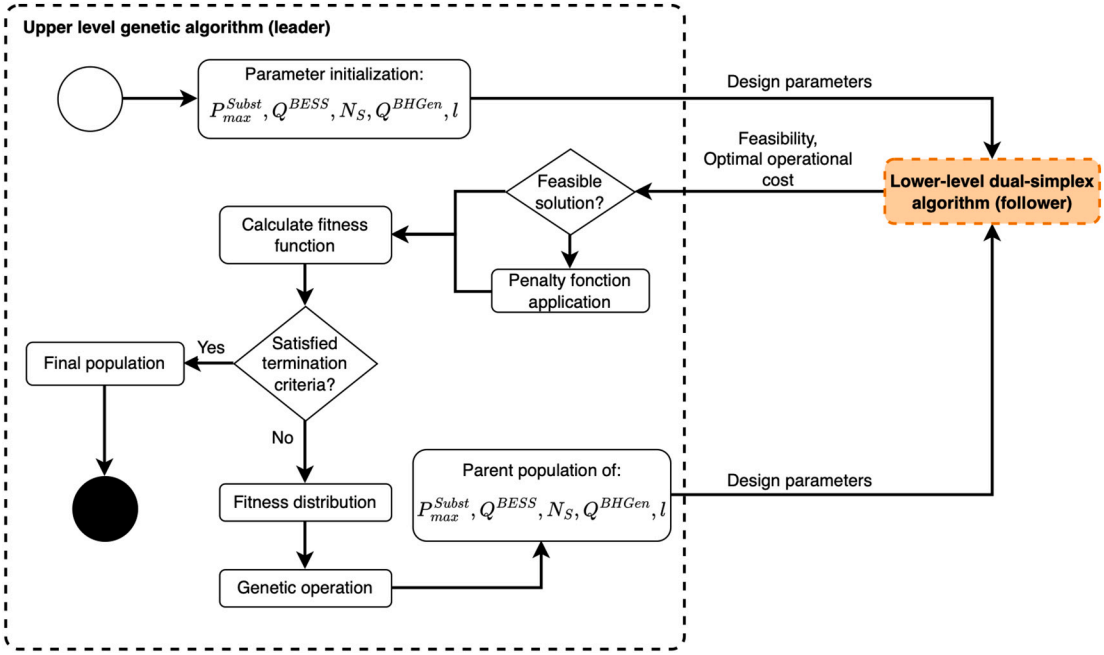

Fig. 6. Upper optimization problem (leader) genetic algorithm flowchart.

lower-level problem returns infeasible solutions, the penalty function is applied. If the termination criteria are not satisfied, the GA algorithm evaluates the normalized non-dominated solutions with the fitness distribution. Then, the algorithm performs genetic operations (crossover, mutation, etc.) to find the parent population that is fed again to the fitness function. The process is repeated till the termination criteria are met, which will provide optimized solutions in a reasonable amount of time.

2.3.2. Follower: shore power system operator problem (operators)

The objective of the shore power system operator is to minimize the operating cost of the shore power system by finding the power dispatch that reduces the cost of electricity and power for the port. In practical applications, the shore power system operator will use a real-time EMS that will do the power dispatch between the energy sources. However, in this study, the algorithm needs to find the optimal power dispatch that the shore power system EMS would achieve. To do so, the lower-level receives in its inputs the parameters of ships electrical demand, and the decision variables generated by the GA algorithm of the upper-level: P_{max}^{Subst}, Q^{BESS}, N_S, Q^{BHGen}, and l.

For the BESS and electrical substation, the objective function is (32):

$$C_{(d,m)}^{Elec\ opt}\left(P_{(b,t,m)}^{SP}\right) \in \underset{P_{(b,t,m)}^{SP}}{arg\min} \sum_{t=1}^{T}\left(C^{ElecSP} \times P_{(t,m)}^{Subst} + C^{PowerGrid} \times P_{(b,t,m)}^{SubstPeak}\right)$$
$$s.t., (1), (2), (3), (4), (5), (6), (7), (8), (9), (10), b \in B^{Subst}, and$$
$$\sum_{b \in B^{Subst}} P_{(b,t,m)}^{SP} = P_{(t,m)}^{Subst} + P_{(t,m)}^{B} \tag{32}$$

where T is the set of time $t \in T$, m is the month, and berth $b \in B^{Subst}$, B^{Subst} is the set of berths that are connected to the distribution network.

For the mobile hydrogen generator, the objective function is (33):

$$C_{(d,m)}^{H\ opt}\left(P_{(b,t,m)}^{SP}\right) \in \underset{P_{(b,t,m)}^{SP}}{arg\min} \sum_{t=1}^{T}\left(C^{H} \times P_{(t)}^{FC} \Big/ \eta_{eff} \bullet \frac{3.6MJ/kWh}{119.96MJ/kg}\right)$$
$$s.t., (3), (4), (5), (6), (7), (8), (9), (10), (11), (12), (13), (14), (15), (16), b \in B^{HGen}, and$$
$$\sum_{b \in B^{HGen}} P_{(b,t,m)}^{SP} = P_{(t,m)}^{FC} + P_{(t,m)}^{BHGen} \tag{33}$$

where $b \in B^{HGen}$, B^{HGen} is the set of berths that are supplied by the mobile hydrogen generator.

Therefore, the optimization algorithms return the results to the upper optimization problem. The objective functions of the shore power system operator problems and their constraints are linear or can be linearized. The optimization problems can be solved with linear programming (LP) techniques as detailed by the work of Antunes et al. [35]. Fig. 7 presents the flowchart of the dual-simplex algorithm utilized to solve the follower problem followed by the detailed description of the algorithm.

The GA-generated design parameters from the shore power system designer are evaluated month-by-month to capture annual operational variability and seasonality. For each step, the solver first preprocesses the model: it enforces variable bounds, detects linear inequality and equality constraints, checks consistency of bounds and constraints, and

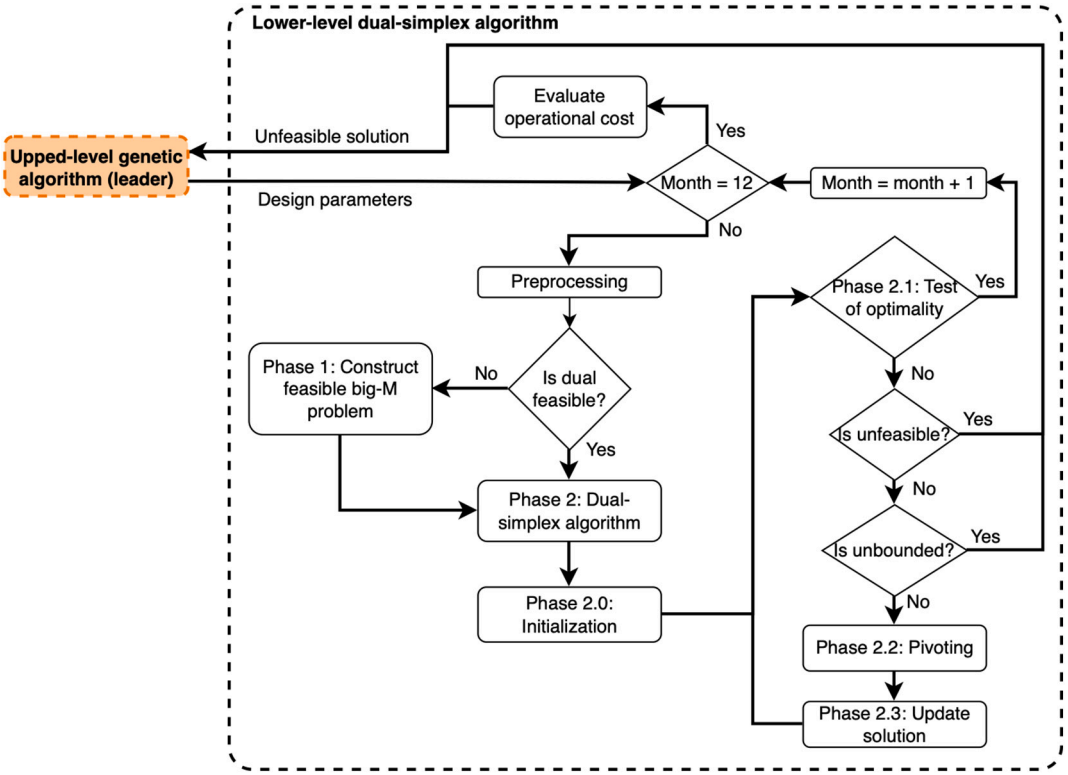

Fig. 7. Dual-simplex algorithm flowchart.

converts inequalities to equalities by introducing slack variables. Initial feasibility is then assessed on the dual problem. If the dual is infeasible, a big-M reformulation (adding slack or penalty terms) is applied to obtain a feasible dual. Phase 2 applies the dual-simplex method to seek optimality: pivoting and solution updates continue while improving neighbouring points and maintaining feasibility. If the algorithm fails to converge within the maximum iteration threshold, the candidate is declared infeasible. The dual-simplex workflow and flowchart follow the formulation in [36].

Once all optimal power dispatch of P^{Subst}, P^{BESS}, P^{FC}, and P^{BHGen} for all t and all month m is found, the annual cost of operation is calculated and sent to the upper optimization problem.

3. Results and discussions

Using a realistic port layout as a test case, the proposed approach intends to determine the best design to maximize the profits of the port while ensuring minimal operational costs. The work of Daniel et al. [37] was evaluated to propose a typical dry bulk port that would be well suited for the test case, including berth utilization, and the physical layout and distances. Notably, the considered study addressed the dry and liquid cargo shipping network of the St. Lawrence and Great Lakes. Nevertheless, investigating a container, cruise, tanker, and other types of terminals is also feasible by adapting the layout configuration and input parameters. The cost parameters used in the test cases are summarized in Table 1.

Table 1
Value of cost parameters in USD.

Symbol	Definition	Value
C^{Bat}	Battery cost in [$/kWh] [38]	300
C^{Dist}	Cost of the distribution network in [$/m] [39]	275
C^{ElecSP}	Cost of electricity sold to the ship in [$/kWh] [40]	0.1125
$C^{ElecGrid}$	Cost of electricity from the grid [$/kWh] [41]	0.03019
C^{FC}	Cost of the hydrogen generator multi-stack fuel cell in [$/kW] [42]	142.5
C^{Htruck}	Cost of the hydrogen truck in [$] [43]	200,000
C^{Htank}	Cost of the hydrogen tank in [$] [30,42]	175,000
C^{H}	Cost of hydrogen [$/kg] [44]	4.00
$C^{PowerGrid}$	Electrical cost of power of the substation in [$] [41]	11.5695
C^{SPop}	Ship cost per shore power connection in [$] [45]	575
C^{Subst}	Variating cost of the substation in [$/kW]	333
C^{Subst}_{base}	Fixed cost of the substation in [$]	7.5
C^{CMS}	Cost of the cable management system in [$]	187,500
I^{SPop}	Income of the charges per ship connection in [$]	375
i_r	Interest rate in [%]	6
N	Total project recovery period in [y]	25

The berth layout of Fig. 8 presents the five different berths of the terminal that are considered in this test case. Berths No. 1 and 2 are at a grain elevator, berths No. 3 and 4 are break bulk, and berth No. 5 is a remote dry bulk berth. The yearly usage of berths No. 1 to 5 is 3%, 25%, 22%, 15%, and 1% respectively, with a distance of 400 m between berths No. 1 and 2, 400 m between berths No. 2 and 3, 200 m between berths No. 3 and 4, and 600 m between berths No. 4 and 5. The typical daily power demand of the ships at berth is presented in Appendix B. Finally, the model evaluates the test case parameters in the MATLAB environment.

3.1. Test case optimal results

The results of the optimization indicate that the optimal system has one substation connected to berths No. 2, 3, and 4 and that berths No. 1 and 5 are supplied by one mobile hydrogen generator. This layout was found by the algorithm to be the optimal choice to reduce the total costs including the investment and the operations. The proximity of the berths had an impact on the results as a remote berth is more expensive to connect to the electrical distribution network. Berth utilization was also a significant contributing factor. Berths No. 1 and 5 are far and less utilized than the other ones resulting in a logical decision by the algorithm to supply them with the hydrogen generator.

Fig. 9 displays the results in bar graphs and a pie chart in terms of total CAPEX, total annual CAPEX, and total OPEX.

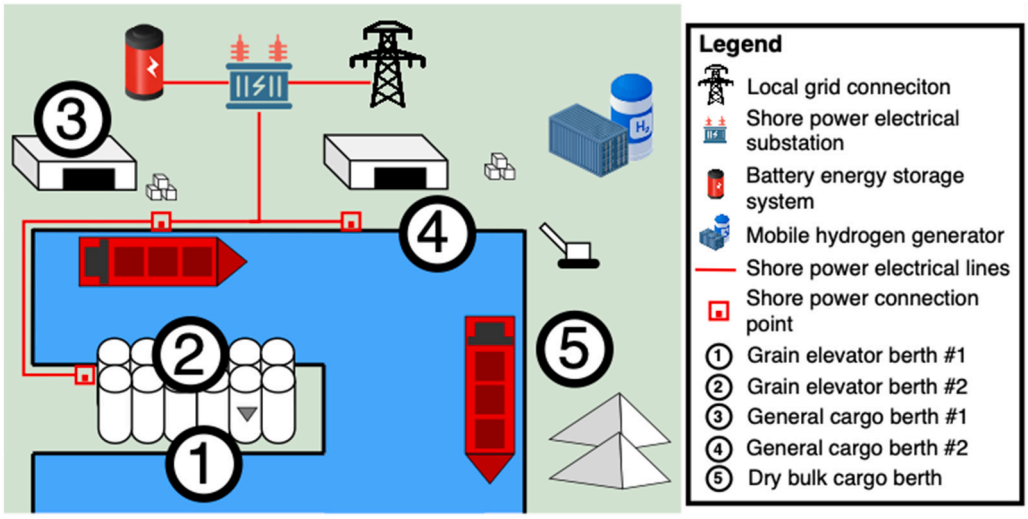

Fig. 8. Test port area with berth number.

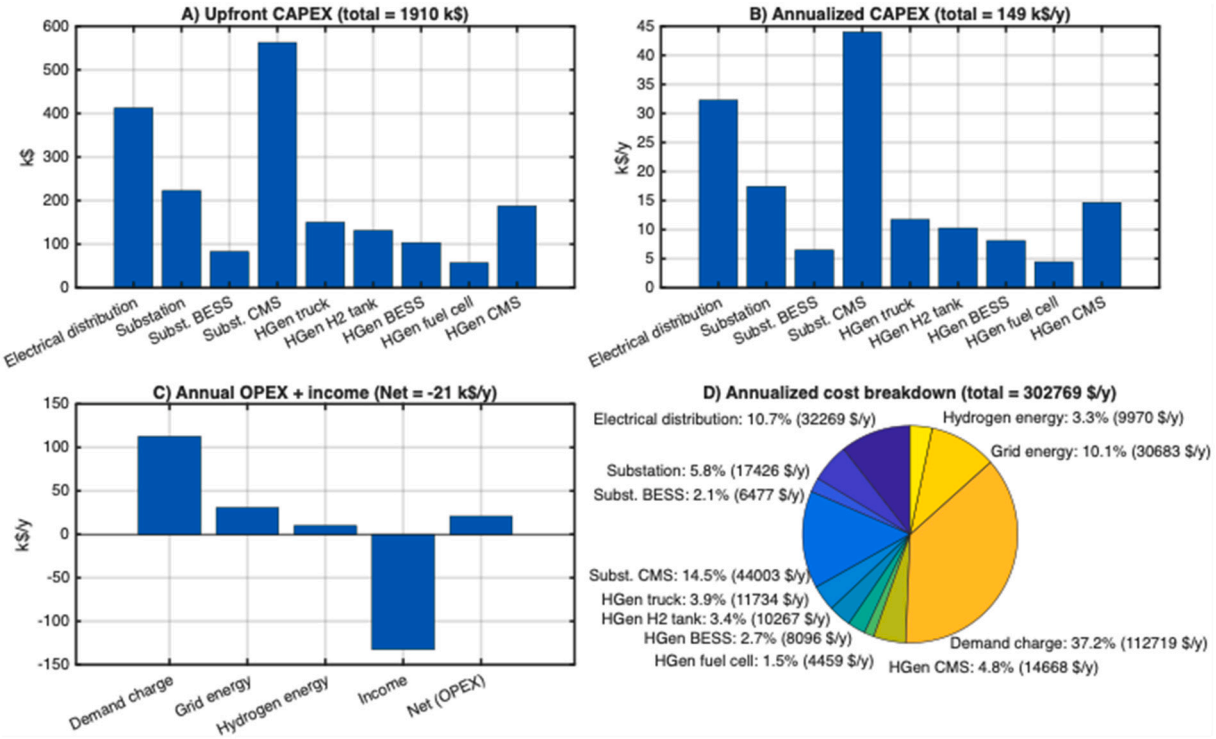

Fig. 9. Breakdown results for the test case in USD: A) the total capital expenditure for each component, B) the annualized total capital expenditure for each component, C) the total operational expenditure for each expense and income, and D) the pie chart breakdown of the annualized costs.

The breakdown figures show that the demand-charge is the dominant contributor in annualized costs, representing 37.2% of total annual costs. The next largest terms are the cable management system, the electrical distribution network annualized CAPEX at 14.5% and 10.7% respectively, and grid energy purchases at 10.1%. By contrast, the annualized contributions of the substation, the BESS, the hydrogen-generator battery, fuel cells, and hydrogen fuel are comparatively smaller at 5.8%, 2.1%, 2.7%, 1.5%, and 3.3% respectively. The results also indicate that no replacement of the batteries or fuel cells was required because of the low utilization rate of the equipment.

Then, Table 2 presents the numerical results from the test case and their related levelized cost of energy values.

A total investment of $1.28 M is required to build the substation, build the electrical distribution network, purchase the CMS, purchase the transformer, and purchase the BESS. It results in a levelized cost of electricity (LCOE) of ¢11.02/kWh for the investment. The LCOE of the electricity itself is constant at ¢3.38/kWh and reaches ¢12.40/kWh for the cost of power. Therefore, the costliest expense for the substation is the cost of power.

Even with the income from the electricity sold to the ship and the connection fee, the total substation LCOE, hydrogen generator LCOE, and annual profit are negative at -¢12.95/kWh, −¢114.11/kWh, and -$170 k respectively. The cost difference with a zero-profit scenario represents 56% of the total annualized CAPEX and OPEX, and could be funded by governments or by increasing the cost of electricity and the connection fee for the ship.

Table 2
Results for the test case in USD.

Variable	Result
Design parameters	
Substation maximum budgeted power	891 kW
BESS capacity	367 kWh
Hydrogen generator multi-stack fuel cell system maximum power	400 kW: 4 stacks of 100 kW
Hydrogen generator battery capacity	460 kWh
Number of mobile hydrogen generator	1
Capacity of the hydrogen generator fuel tank	1000 kgH_2
Substation costs (including distribution and the BESS)	
Total CAPEX	$1,280,332
Annualized CAPEX	$100,156
Annual OPEX	$143,416
Resulting levelized cost of electricity	¢3.38/kWh
Resulting levelized cost of power	¢12.40/kWh
Resulting levelized cost of investment	¢11.02/kWh
Electricity and connection incomes	¢13.85/kWh
Mobile hydrogen generator costs	
Total CAPEX	$629,250
Annualized CAPEX	$49,224
Annual OPEX	$9969
Resulting levelized cost of operation	¢21.66/kWh
Resulting levelized cost of investment	¢106.96/kWh
Electricity income	¢14.51/kWh
Total annual profit	-$170,209

The maximum budgeted power of the substation is found to be 891 kW, and a BESS capacity of 367 kWh. The total power of the substation is not the real maximum power because a contingency security factor is added at the engineering design stage. However, it represents the maximum budgeted power that the substation should be operated to optimize the operational costs. Indeed, one of the important operation cost components is the peak power demand that is supplied by the grid. Fig. 10 below presents a day in the simulated year to show how the BESS is able to compensate for the constrained substation and limit the total power requested to the grid.

The x-axis of Fig. 10 is the time over 24 h, the left y-axis is the power in kW, and the right y-axis is the battery SOC in percentage. The pink curve represents the power demand of the ships using shore power. The blue curve represents the power of the battery, and the dotted blue curve presents its state of charge. The green line is the power of the substation.

Fig. 10 shows that the BESS was able to diminish the maximum power requested to the grid by maintaining it at a maximum level, thus reducing the electrical cost of power. The work of the BESS is seen by the variations of power on P^{BESS}, which compensate for the substation high demands constrained by the substation budgeted maximum power. At the end of the day, the state of charge of the BESS comes back to its initial value successfully.

For the mobile hydrogen generator, an investment of $629 k covers the hydrogen truck, hydrogen tank, the 400 kW multi-stack fuel cell system, and the 460 kWh battery. The resulting LCOE for the operations reaches ¢21.66/kWh, and the investment is ¢106.96/kWh. This result is high because the mobile hydrogen generator has a much lower utilization rate than the substation. On the other hand, the levelized income at ¢14.51/kWh is slightly higher than that of the substation because the connection fee is spread among fewer kWh of utilization.

The results also indicate a daily hydrogen consumption of about 236 kg. Therefore, the 1000 kg hydrogen fuel tank would be sufficient to cover the power demand of a bulk carrier at berth for 3–4 days, which is the world average time that bulk carriers spend in ports [46].

Similar to Figs. 10, 11 and 12 show how the mobile hydrogen generator multi-stack fuel cell system and battery supply the ship for a typical day. When the power is at zero, it is because the ship has stopped or has not yet started to use shore power.

The figures show that the same mobile hydrogen generator can supply different ships and different power demands. Because the system only supplies one ship at a time, there are fewer power variations than on the substation and the BESS. The battery takes a minimum share of the load because fuel cells cannot supply high-frequency variations of the load. Therefore, the battery needs to be recharged regularly. At the end of the day, the battery needs to successfully regain its initial state of charge as bulk carrier port calls can last multiple days.

From a policy perspective, the cost structure suggests differentiated levers: investment subsidies reduce infrastructure-driven annualized CAPEX, notably for the electrical distribution network and substation. Then, operational support mechanisms, such as demand-charge mitigation or dedicated shore power tariffs, could target the dominant demand-charge term. Carbon policies can further improve revenue adequacy by increasing the relative attractiveness of shore power versus onboard diesel generation, enabling higher cost recovery through electricity sales and connection fees.

3.2. Test case sensitivity analysis

A sensitivity analysis was performed in Appendix C to see how the model reacts to variations of multiple parameters. It concludes that the model outputs are proportionally related to its inputs for variations of ±100%, with variations in the grid electrical costs, ship electricity cost, and substation investment cost being the most sensible parameters. This sensitivity analysis enabled to reinforce the robustness of the method

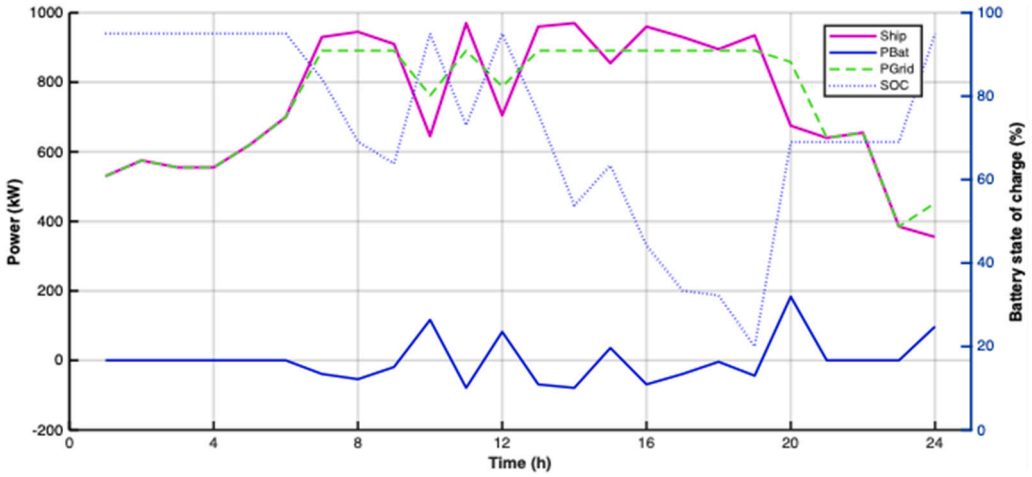

Fig. 10. Power dispatch of the electrical substation connected to berths No. 2-3-4 and the battery energy storage system for a typical day in December.

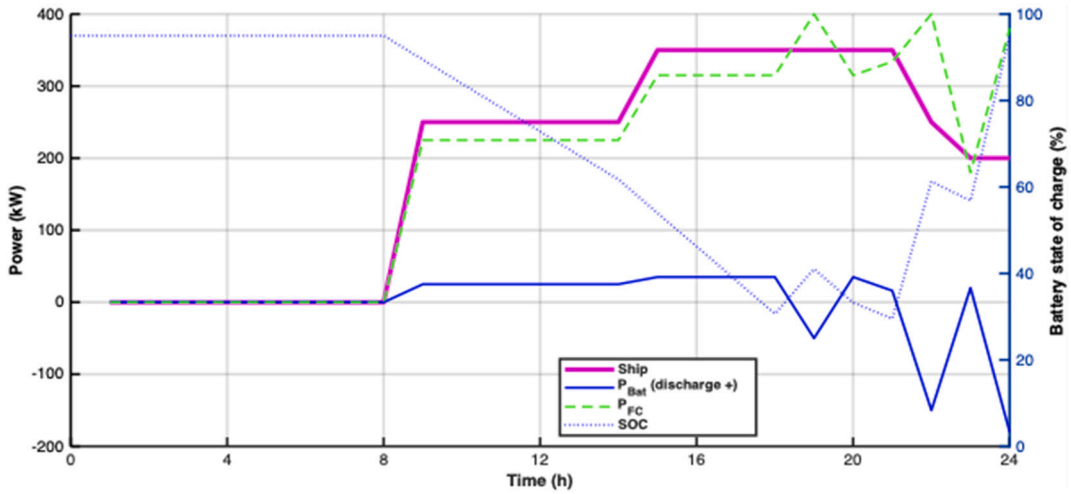

Fig. 11. Power dispatch of the hydrogen generator for berth No. 1 for a typical day in December.

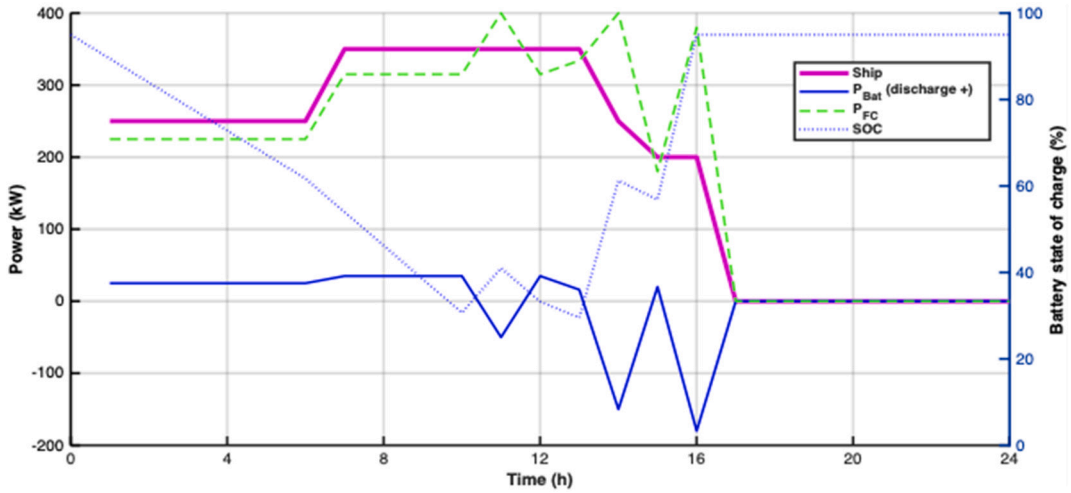

Fig. 12. Power dispatch of the hydrogen generator for berth No. 5 for a typical day in December.

and show the impact of parameter variations on shore power system design. However, the variation of berth utilization is another critical parameter that is unknown and might be subject to higher variations. For instance, the number of shore power-equipped ships is in constant evolution. Therefore, a deeper analysis of berth utilization has been conducted to assess the economic impacts of the system under low utilization scenarios.

Fig. 13 presents the levelized cost (y-axis) based on the variation of the total capacity utilization rate of the installation (x-axis) to see the relationship between different scenarios on the same basis. The total capacity utilization is measured as the quantity of energy that can be supplied by the electrical substation or the hydrogen generator to the ships. Therefore, it indicates how sensible the economics of the solution are to different utilization rates.

The green dotted curve represents the LCOE of the substation if no BESS was used, but with only berths No. 2, 3 and 4 connected as per the results of the reference scenario of Section 3.2. Then, the grey dashed curve is the LCOE of the reference scenario, but considering that the ships coming to the port do not have a peak power demand, and where the average power is equal to the peak power demand. This case is investigated to see if the BESS is economic even in cases of ships having constant loads. The blue solid curve presents the LCOE of the reference optimal scenario with the BESS and the berths No. 2, 3 and 4 connected. The orange curve presents the LCOE of the mobile hydrogen generator and is shorter than the other curves as only one hydrogen generator cannot supply the same quantity of energy as the electrical substation can. The black dotted curve is the income from electricity sold to the ships, and the triangles show the current operation point based on the test case parameters.

Finally, two scenarios without hydrogen generators are investigated. They are used as a reference to compare the effectiveness of the mobile hydrogen generator solution with the other solutions. The pink dashed curve presents the case where all berths would be connected to the electrical substation and where the BESS is optimal to reduce costs. The light blue dashed curve is the case where all berths would be connected to the electrical substation, but without any BESS system. The light blue scenario is the equivalent of current shore power deployment strategies without BESS or mobile hydrogen generators.

Fig. 13 shows that a variation in the utilization of the substation close to its actual utilization point would not affect the LCOE very much. However, if it is not used enough, the LCOE can increase significantly. Therefore, the port needs to ensure that a minimum number of ships will connect. However, variations in the mobile hydrogen generator utilization will always affect the costs because of the steep slope at the real set point. While a high utilization could reduce the LCOE tremendously, it is not able to reach the substation LCOE partly because of the higher resulting cost of electricity generated with hydrogen and investment cost.

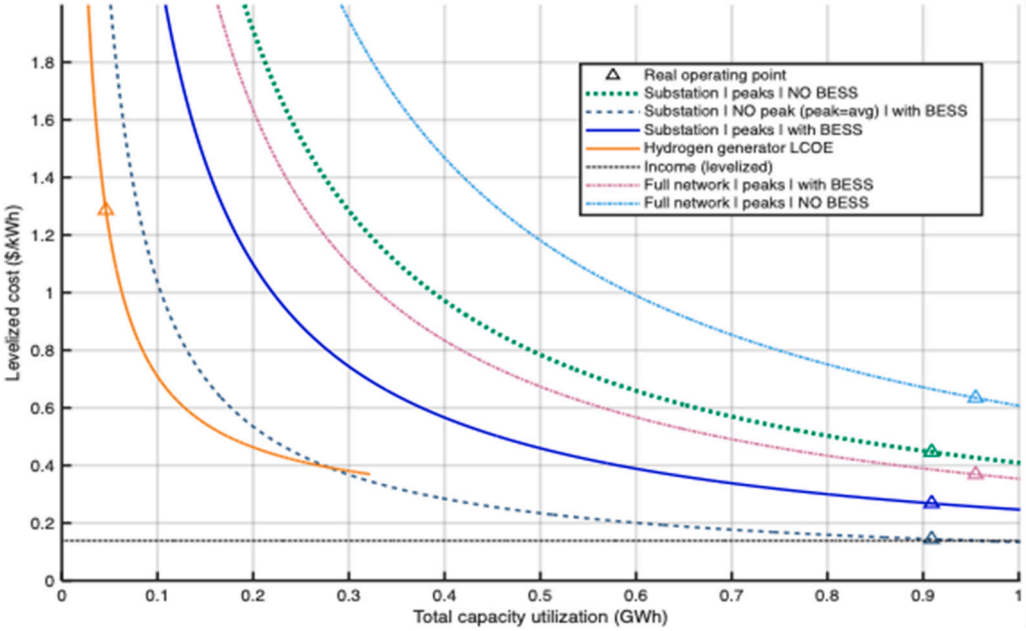

Fig. 13. Sensitivity of the levelized cost on utilization.

Also, the graph shows that the relation between the LCOE and the berth utilization is an exponential inverse. Therefore, the LCOE diminishes quickly at the beginning and flattens after about 500 MWh of utilization, which is ~6% usage of the substation capacity. It means that bulk carriers' shore power terminals need minimal usage to ensure they are operated economically. For comparison, the real operating point of the reference scenario is at 11.8% usage of the total substation capacity.

The gap between the mobile hydrogen generator curve and all other curves shows that, even if expensive, the mobile hydrogen generator enables the reduction of the total costs of the marine green port by preventing the costly installation of underground cables for low-utilization berths. Indeed, the mobile hydrogen generator achieves the same LCOE but with 43%–90% less supplied energy, i.e., less effective electrical utilization, depending on the scenario.

Then, the gap between the solid blue curve (reference optimal scenario) and the green curve (no BESS) shows a cost difference of about 69%. It confirms that the BESS is effective in optimizing the profit of shore power under demand-charge electrical tariffs. Also, the low LCOE

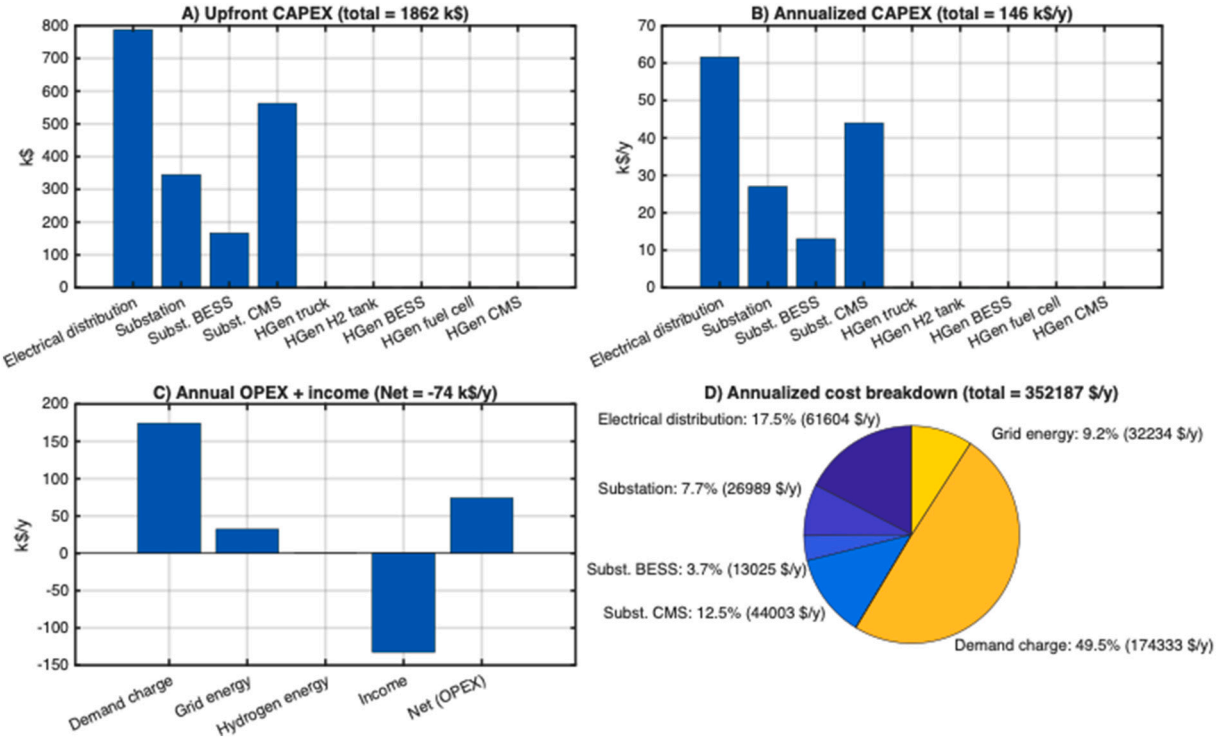

Fig. 14. Breakdown results for full network test case in USD: A) the total capital expenditure for each component, B) the annualized total capital expenditure for each component, C) the total operational expenditure for each expense and income, and D) the pie chart breakdown of the annualized costs.

of the dashed grey curve indicates that ships without peaks provide the best profits for the port.

Then, the reference optimal scenario (blue solid curve) presents better results in all cases when compared with the two full network scenarios: 63% reduction with the pink dashed curve and 79% reduction with light blue dashed curve. It shows the importance of BESS and mobile hydrogen solutions to democratize shore power in zero-emission ports. Then, the gap between the full network scenario with BESS (light blue dashed curve) and the full network scenario without BESS (pink dashed curve) highlights that the BESS are essential to reduce total costs even in conventional shore power deployment strategies. The latter solution requires larger electrical installations to cover the peak power demands of the ship cranes or other electrical loads on the ships. Also, the maximum power requested from the grid cannot be reduced, reinforcing the need for a BESS to lower the demand-charge cost of power.

The full network scenario with BESS was further investigated. Fig. 14 reports the corresponding cost-composition breakdown using the same representation as the reference optimal test case.

Compared with the hybrid configuration, the full-network case requires higher grid-facing sizing (P_{max}^{Subst}=1380 kW; $Q^{BESS} = 740$ kWh) and is more exposed to demand-charge costs. Demand-charges dominate the annual cost with 49.5% of annual total costs and distribution-network annualized costs increase, 17.5%, resulting in lower profitability under the demand-charge tariff and supporting mobile hydrogen generation as a cost-mitigating option for remote or low-utilization berths. The final total profit is 29% higher than the reference hybrid scenario, showing the importance of mobile generation solutions for remote and low-utilization berths.

3.3. Model sensitivity and limitations

To further assess sensitivity to external drivers and to validate the proposed optimization framework, additional analyses were conducted in Appendix D on model optimality, electricity-pricing schemes, and berth-utilization scenarios. The results indicate that the suggested metaheuristic model is efficient in finding near-optimal results in a reasonable amount of time. Also, both tariff structure and berth-utilization patterns strongly influence the optimal topology and sizing, with demand-charge exposure emerging as the dominant factor influencing profitability. Among all tested cases, only the high-utilization scenario with 40% utilization at all berths yields the best annual profit at -$135 k, highlighting that high berth usage is critical for cost recovery in the analyzed context.

The proposed model remains subject to several limitations. First, the results are highly dependent on the specific characteristics of the analyzed port terminal: berth layout geographical configuration, electrical distribution, and berth-utilization patterns. They may lead to substantially different optimal topologies and sizing outcomes. Second, several technical and economic components are represented using simplified assumptions, including fuel-cell and generator efficiency, battery sizing procedures, load-demand characterization, and electricity tariff structures, which could be refined through higher-resolution operational data and more detailed techno-economic sub-models. In addition, ship-type differences and operational variability are not investigated. Finally, the current framework is well suited for demand-charge tariff, but needs to be adapted to other types of energy tariffs. Therefore, while the framework is generalizable, the present test case can be adapted and calibrated with diversified real-world datasets to ensure robust applicability and to demonstrate optimal performance across a broader range of terminal types and operating conditions.

4. Conclusion

This study developed and validated a bilevel optimization framework for the joint design and operation of shore power connection systems integrating battery energy storage systems and mobile hydrogen generators. The proposed bilevel architecture captures the hierarchical interaction between shore power investors and system operators by coupling a genetic algorithm for infrastructure sizing and distribution layout with a dual-simplex linear power dispatch algorithm.

Applied to a representative five-berth bulk terminal, the model identified an optimal hybrid configuration consisting of an 891 kW substation, a 367 kWh BESS, and one 400 kW mobile hydrogen generator with a 460 kWh battery. Compared with conventional full-network electrification without storage or mobile generation, the optimized configuration reduced total system costs by up to 63–79%, depending on the reference scenario. The BESS significantly reduced exposure to demand-charges by limiting peak grid power, while the mobile hydrogen generator avoided costly electrical-distribution extensions for remote berths or with low-utilization rates. Despite these improvements, the optimized annual profit remained negative at –$170 k, indicating that bulk terminals with low berth utilization struggle to achieve full cost recovery under current demand-charge tariff structures. To achieve a zero-profit scenario, a subsidy of 56% of the total annual costs is required.

Demand-charges are the dominant contributor to annualized costs in the reference case, accounting for 37.2% of the total. The remaining cost is largely driven by infrastructure-related CAPEX, with electrical distribution and cable management systems forming the next most significant elements, while equipment costs for the substation, BESS, and hydrogen system are comparatively smaller. This cost structure indicates that improving project viability will likely require a dual policy approach. It will be required to provide targeted mitigations of demand-charges through adapted shore power tariffs, and to support infrastructure investments on the shore-side such as electrical distribution and cable handling systems, which are substantial.

From an engineering perspective, the results confirm that hybridizing grid supply with strategically sized BESS and modular hydrogen generators improves flexibility and reduces infrastructure oversizing under the demand-charge electricity tariff. However, economic feasibility remains highly sensitive to berth utilization and tariff design. The utilization sensitivity analysis shows that bulk-carrier shore power installations must be operated above a minimal utilization level of ~6% to keep the LCOE stable against utilization-driven variations.

Future work should further investigate the economic gap between optimized hybrid configurations and breakeven operation by quantifying the required contributions from governments and shipowners under different electricity tariffs. The integration of on-site renewable-powered hydrogen production and additional operational layers, such as berth and quay-crane allocation coupling, could also refine system-level optimization.

Also, the proposed framework is well-suited to demand-charge tariffs of electricity, but it is less adapted to purely energy-based tariffs such as fixed, time-of-use, or day-ahead pricing. Future work should therefore adapt the model to better capture these tariff dynamics and include BESS revenue strategies such as electricity resale to the grid to improve profitability.

Finally, while the lower-level dispatch was validated against a dynamic-programming benchmark, future work should further assess global optimality of the overall bilevel solution by comparing against additional references and methods across a broader set of test cases.

CRediT authorship contribution statement

Hugo Daniel: Writing – original draft, Validation, Software, Methodology, Investigation. **Loïc Boulon:** Writing – review & editing, Validation, Supervision, Resources, Conceptualization. **João Pedro F. Trovão:** Writing – review & editing, Validation, Supervision, Resources, Funding acquisition, Conceptualization. **David Williams:** Writing – review & editing, Resources, Funding acquisition.

Declaration of Generative AI and AI-assisted technologies in the writing process

Not applicable.

Declaration of competing interest

The authors declare that they have no conflicts of interest.

Acknowledgments

This work was supported by the Canada Research Chairs Program (950-230672), by the Mitacs Accelerate Program (IT17570 and IT32307), and in part by Fednav INC. It also received support from FCT, Portuguese Foundation for Science and Technology, under project UIDB/00308/2020 and by the Portuguese Recovery and Resilience Plan (RRP), through project number 56, ATE (*Aliança para a Transição Energética* - 02/C05-i01.02/2022.PC644914747-00000023), and in part by Fednav.

Appendix A

Table 3
Abbreviations and symbols.

Symbol	Definition
Variables and parameters	
β	Share energy that is supplied by the multi-stack fuel cell system
λ	Probability of having a ship at a berth
$\lambda_{Multiple\ ship}$	Probability of having fewer mobile hydrogen generators than ships at berth
λ_{Tresh}	Statistical threshold
Λ	Set of probabilities for the berths that will be supplied by a hydrogen generator
η_{eff}	Factor representing the efficiency of the multi-stack fuel cell system
B^{HGen}	Set of berths that are supplied by the mobile hydrogen generator.
B^{Subst}	Set of berths connected to the electrical distribution network
C_a	Annualized cost
C_a^{BESS}	Annualized CAPEX of the BESS connected to the substation
C_a^{HGen}	Annualized CAPEX of the mobile hydrogen generators
C_a^{BHGen}	Annualized CAPEX of the mobile hydrogen generators' batteries
C_a^{Subst}	Annualized CAPEX of the electrical substation
C_a^{Tot}	Total annual cost
C^{Bat}	Battery cost
C^{Dist}	Cost of the distribution network
C^{ElecSP}	Cost of electricity sold to the ship
$C^{ElecGrid}$	Cost of electricity from the electrical provider
$C^{Elec\ opt}$	Optimal electrical cost for the port
C^{FC}	Cost of the fuel cell
C^{H}	Cost of hydrogen
$C^{H\ opt}$	Optimal hydrogen cost
C^{Htank}	Cost of the hydrogen tank trailer
C^{Htruck}	Cost of the hydrogen truck
C_I^{BESS}	Total investment cost of the substation BESS
C_I^{FC}	Total investment cost of the hydrogen generator's multi-stack fuel cell system
$C_I^{HGen\ Bat}$	Total investment cost of the hydrogen generator's battery
C_I^{Subst}	Total investment cost of the substation
$C^{PowerGrid}$	Electrical cost of power of the substation,
$C^{Power\ opt}$	Optimal power cost
C^{Subst}	Cost of the substation
C_{base}^{Subst}	Base cost of the substation
D^{Dist}	Function of the length of the distribution network for a berth layout l
F	Set of mobile hydrogen generators
i_r	Interest rate
I_a^{Tot}	Total annual incomes
I^{ConnSP}	Total Income of the fees for ship connections to shore power
I^{ElecSP}	Income from electricity sold to ships
I^{SPop}	Port operational income of the ship's connections
L	Set of electrical distribution layout
M	Set of months in the year
mH	Mass of hydrogen
N^{Conn}	Number of ship connections to shore power
N^{Day}	Number of days in a month
N^{HGen}	Number of hydrogen generators
N^{s}	Number of fuel cell stacks
η_{eff}^{Bat}	Efficiency of energy transfer with the battery
η_{eff}^{FC}	Efficiency of the fuel cells
P^{BESS}	Power of the BESS system
p_{max}^{BESS}	Maximum power of the BESS system
P^{BHGen}	Power from the hydrogen generator battery
P^{FC}	Power of the multi-stack fuel cell system

(*continued on next page*)

Table 3 (*continued*)

Symbol	Definition
P^{mFC}	Power of a single fuel cell stack
p^{Grid}	Average power supplied from the grid
P^{HGen}	Power from the hydrogen generator
$Profit_a$	Annualized profits
P^{SP}	Power requirement from the ships shore power connections
P^{Subst}	Power flow that is transferred from the substation to the ships
P^{Subst}_{max}	Maximum budgeted power of the substation
Q^{BESS}	Capacity of the BESS
Q^{HGen}	Energy demand for the mobile hydrogen generators
Q^{BHGen}	Hydrogen generator battery capacity
Q^{SP}	Electrical demand of the ships
Q^{Subst}	Total electrical demand of the substation to the grid
SOC	State of charge
T	Set of hours in the day
z^{BESS}	Binary variables representing the use of the BESS
z^{BHGen}	Binary variables representing the use of the hydrogen generator's battery
z^{FC}	Binary variables representing the use of the hydrogen generator's fuel cells
z^{Subst}	Binary variables representing the use of the substation
Subscript	
a	Annual
b	Berth identifier
d	Day identifier
f	Hydrogen generator identifier
l	Layout identifier
I	Investment
m	Month identifier
max	Maximum
min	Minimum
n	Period of the interest rate
t	Time unit (hour) identifier
Abbreviations	
BESS	Battery energy storage system
CAPEX	Capital expenditure
CMS	Cable management system
CO_2	Carbon dioxide
EMS	Energy management strategy
GA	Genetic algorithm
GHG	Greenhouse gas
LCOE	Levelized cost of electricity
LP	Linear programming
MINLP	Mixed-integer non-linear programming
OPEX	Operational expenditure
TOU	Time-of-usage

Appendix B

The general power demand of the ships at berth for the test case is presented in Figs. 15 and 16. It is based on the real power demand of bulk carriers from the International Maritime Organization power demand of ships [1] and from the work of Daniel et al. [37] addressing the dry and liquid cargo shipping network of the St. Lawrence and Great Lakes. A monthly utilization factor is applied to the typical load profile to ensure it represents a realistic power demand of the ships in function of the season with 50%, 50%, 70%, 80%, 90%, 100%, 80%, 80%, 100%, 100%, 100%, and 70% for January to December.

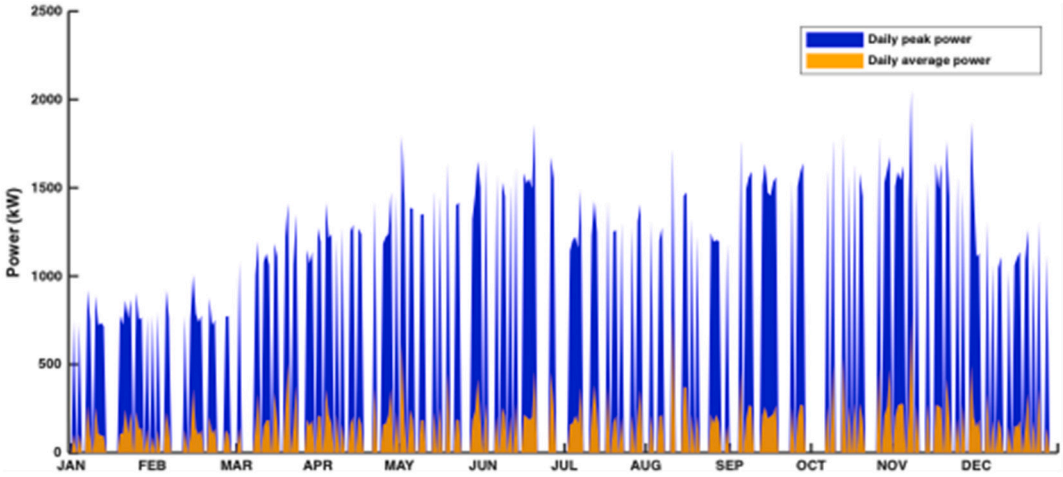

Fig. 15. Estimated annual power demand for the test case dry bulk terminal.

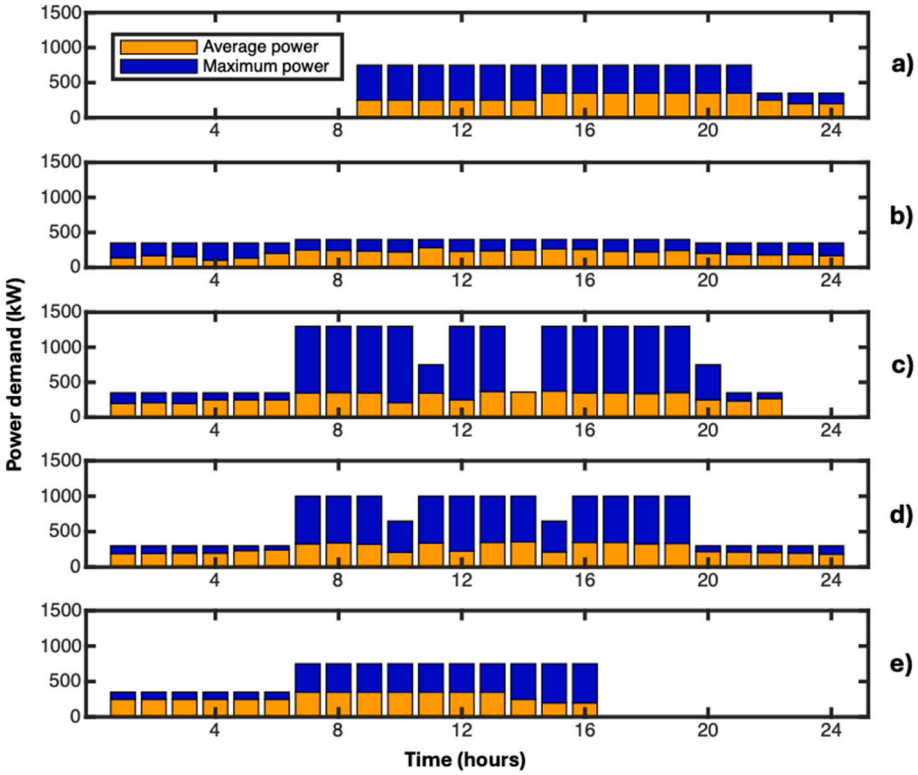

Fig. 16. Typical daily load profile for the five berths of the test case with the first graph at the top representing a) Berth No. 1, b) Berth No. 2, c) Berth No. 3, d) Berth No. 4, e) Berth No. 5.

Appendix C

This appendix discusses the sensitivity of the model outputs to variations in its inputs. Firstly, the input parameters related to investment cost, operational cost, and berth utilization are addressed, followed by the design parameters in a second analysis.

This appendix assesses how sensitive the model outputs are to variations in key input assumptions. The analysis is performed with a one-at-a-time approach: for each sensitivity variable, a discrete set of percentage variations of ±100% is applied around a baseline case (reference scenario), while the genetic algorithm recomputes the optimal design for every scenario.

The different sensitivity variables that are tested are:

Equipment and infrastructure investment costs (CAPEX)

- Substation CAPEX
- Battery energy storage system (BESS) CAPEX
- Fuel cell (FC) system CAPEX
- Electrical substation CAPEX
- Mobile hydrogen generator CAPEX

Operational costs and revenues (OPEX)

- Grid electricity OPEX (energy and demand-charges)
- Ship-side OPEX/revenue assumption (electricity cost paid by ships/income to the port)
- Hydrogen operational cost (fuel and refuelling)

Operational conditions at the port

- One berth load profile variable per berth (Load 1 to Load 5)
- Peak demand assumptions at each berth (Peak 1 to Peak 5)
- Berth utilization factors variable per berth (UTL 1 to UTL 5)

Fig. 17 shows the variation of annual profit as a function of the input perturbation applied to each sensitivity variable. The x-axis reports the input variation in percentage relative to the baseline (−100% to +100%), and the y-axis reports the corresponding profit variation in percentage relative to the baseline profit. Each curve represents one sensitivity variable and connects the tested variation points. The colour and marker in the legend identify the sensitivity variable, while the dashed reference lines at 0% indicate the baseline case (no variation and no change in profit). Because each point corresponds to a full GA re-optimization, the plotted response reflects both the direct impact of the parameter and the design adjustments made by the optimizer.

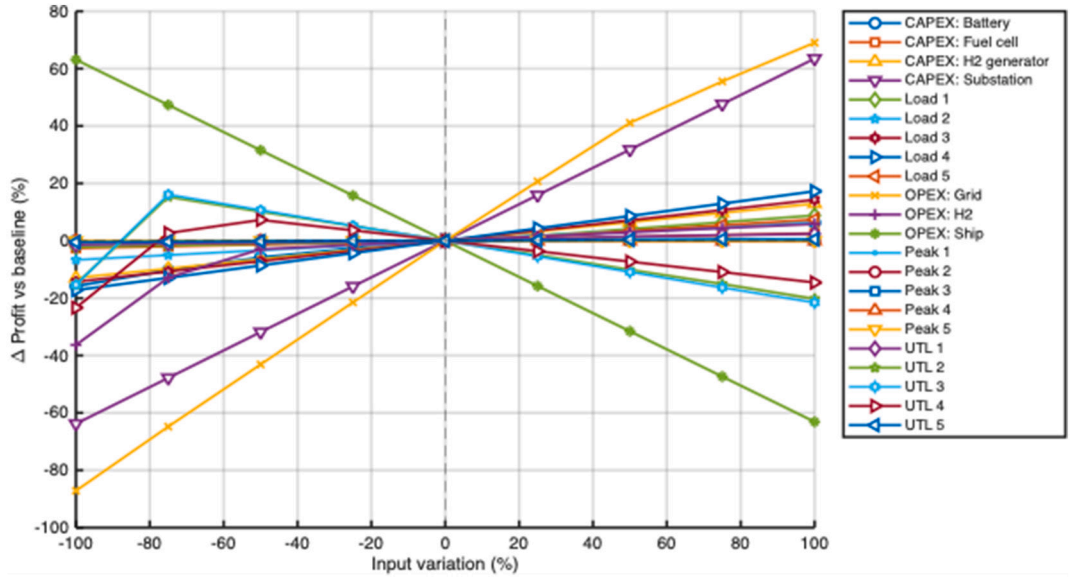

Fig. 17. Sensitivity of the annual profit.

The results from Fig. 17 indicate that the main variables influencing the annual profit sensitivity are the electricity-related OPEX (energy and demand-charges), the ship-side OPEX/income (electricity cost or revenue recovered from ships), and the substation CAPEX. A positive and negative variation of 100% of ship income and substation cost results in a profit variation of roughly −60% to +60%. Variations in grid OPEX exhibit an asymmetric response: a +100% variation can increase profit by approximately +60%, whereas a −100% variation decreases profit by about −80%. Overall, small individual variations of most parameters have a limited influence; however, simultaneous unfavourable changes across multiple parameters could lead to significant deviations in profitability, implying that robust investment decisions should consider combined uncertainty rather than isolated perturbations.

Fig. 18 complements Fig. 17 by providing a ranked comparison of sensitivity variables based on their profit impact at the most negative and most positive tested variations. For each variable, two horizontal bars are plotted: the left bar corresponds to the negative extreme variation (i.e., −100%) and the right bar corresponds to the positive extreme (i.e., +100%). The x-axis shows the profit variation in percentage relative to baseline, while the y-axis lists the sensitivity variables sorted by the maximum absolute impact. This figure is intended to quickly identify which uncertainties matter most for decision-making and whether their impacts are symmetric (similar magnitude on both sides) or asymmetric (large downside risk with limited upside, or the opposite).

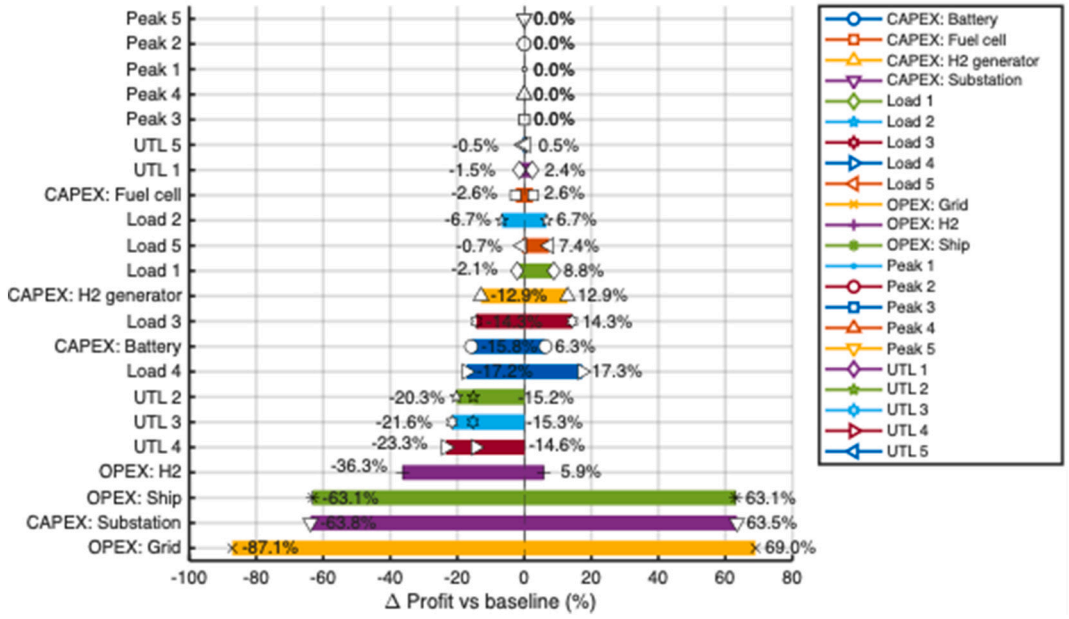

Fig. 18. Sorted sensitivity of the annual profit variation between minimal and maximal variations.

Fig. 18 highlights that, when a BESS is present, variations in peak power assumptions have a relatively low impact on profit. This behaviour is consistent with the modelling assumption that the battery can absorb short-duration peaks effectively. At this stage, the model does not impose a maximum admissible instantaneous peak limit for the BESS response. Therefore, applications with extreme peaks relative to mean demand may require additional constraints. More broadly, Fig. 18 shows that most variables yield larger negative profit deviations than positive gains, indicating that shore power economics are more vulnerable to adverse parameter changes than they benefit from favourable ones. The only larger positive impacts observed correspond to increased load at berths 1 and 5, which are supplied by the mobile hydrogen generator: higher demand increases delivered energy and revenues, whereas lower load produces limited benefit.

Fig. 19 reports the optimal design variables returned by the GA for every sensitivity run using actual variable values (not normalized percentages). The x-axis corresponds to the scenario index (each index is one sensitivity run), and each subplot represents one design variable: the maximum budgeted substation power P_{max}^{Subst}, the BESS capacity Q^{BESS}, the number of stacks in the multi-stack fuel cell system N_S, the hydrogen generator battery capacity Q^{BHGen}, and the electrical distribution layout: l. Bars are colour-coded by the sensitivity variable being perturbed, and the shade of each bar encodes the magnitude and sign of the input variation (lighter tones for negative variations and darker tones for positive variations relative to the 0% case of the perturbed variable). Marker symbols on the bars further distinguish which sensitivity variable is active for a given run, improving readability when several colours are visually similar.

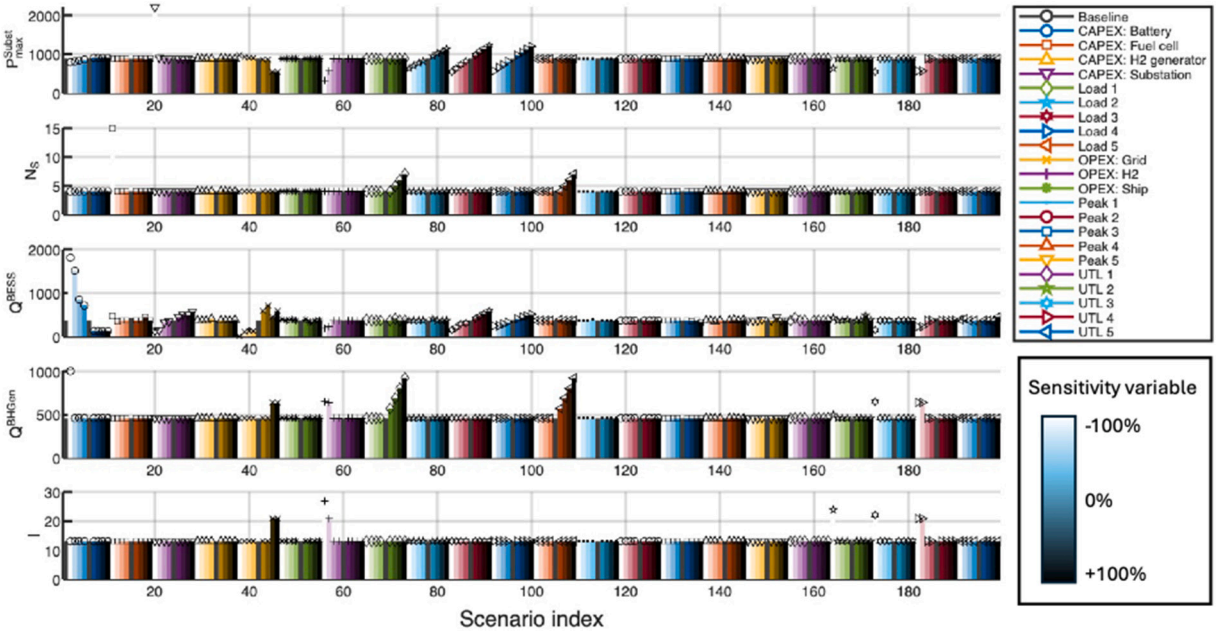

Fig. 19. Sensitivity of the design variables for: the maximum budgeted power of the electrical substation, the electrical substation battery capacity, the maximum power of the mobile hydrogen generator multi-stack fuel cell system, the hydrogen generator battery capacity, and the berth layout identification number.

Fig. 19 shows that load variations on berths 2–3–4 (served by the

electrical substation) strongly affect the optimal P_{max}^{Subst}, as higher substation utilization (Utl 3–4-5) directly drives required grid capacity. The substation BESS capacity Q^{BESS} is primarily influenced by battery capacity cost variations, reflecting the trade-off between storage investment and operational value.

On the hydrogen side, N_S and Q^{BHGen} are impacted mainly by load variations on berths 1 and 5 and not that much by utilization or peak variations. Since these berths are supplied by the mobile hydrogen generator, higher demand increases the required onboard generation and buffering power.

In contrast, the distribution layout identifier l remains stable in most conditions, but varies when high variations of grid electricity cost, hydrogen cost or utilization are present. Layout changes are predominantly driven by utilization variations, which can shift the optimizer to occasionally connect berth 1 or 5 to the electrical substation.

In conclusion, the sensitivity analysis indicates that the model is relatively stable under moderate one-at-a-time perturbations for most inputs, but it is highly sensitive to ship-related revenues and electricity operational costs.

Appendix D

This appendix has the objective to provide more detailed evaluations of the algorithm optimality performances compared with a central single-level optimization model, the lower-level algorithm optimality analysis, and with different electrical pricing tariffs impact on the results.

Central single-level optimization

First, the bilevel model was reformulated over a centralized single-level optimization model to compare the performance of both models. However, modelling an equivalent fully centralized algorithm without substantial simplification and remodelling would require optimizing on the order of hundreds of coupled variables at once (5 upper-level design variables plus 2×24 variables for the power dispatch, monthly for one year, for the lower-level dispatch problems).

As this formulation is impractical, the upper-level was simplified by replacing the interaction with the lower-level by a simple inequality function. Thus, no operation optimization is done on a lower level.

The battery sizing is based on IEEE 485-2020. However, only the high-level battery sizing procedures were considered: supply autonomy time, peak power demand, total capacity, etc. The simplified model also requires the satisfaction of the constraints (34), (35), (36), and (37) for the BESS:

$$Q_{BESS}^{Target} = \left(\max\left(P_{(b,t,m)}^{SP}\right) - P_{max}^{Subst}\right) * N_{AH} \tag{34}$$

$$Q_{BESS}^{Nominal} = \frac{Q_{BESS}^{Target}}{DoD * DM} \tag{35}$$

$$Q^{BESS} \geq Q_{BESS}^{Nominal} \tag{36}$$

$$Q_{BESS}^{Target} \leq \sum_{b \in B^{Subst}} P_{max}^{Subst} - P_{(b)}^{SP} \tag{37}$$

where Q_{BESS}^{Target} is the targeted useful capacity range of the BESS, N_{AH} is the number of hours of autonomy of the battery, $Q_{BESS}^{Nominal}$ is the total capacity of the BESS, DoD is the useful capacity range, DM is the design margin.

A DoD of 75% is chosen to limit short battery aging, and conservative values of 1 h and 10% are used for the number of hours of autonomy and for the design margin respectively.

For the hydrogen generator, the targeted hydrogen generator battery capacity formula (38) is modified to respect (15).

$$Q_{BHGen}^{Target} = \sum_{b \in B^{HGen}} \beta \times \left(P_{(b)}^{SP} - P_{max}^{FC}\right) \tag{38}$$

Then, the central single-layer model is compared with the bilevel reference model in Table 4. The central-level model has a very similar architecture, but feasibility and optimality are not ensured. Nevertheless, the central single-level model enables the evaluation of the high-level performance of the bilevel approach.

Table 4
Comparison between the centralized single-level and the bilevel algorithms.

Variable	Proposed bilevel model	Central single layer model
Design parameters		
Substation maximum budgeted power	891 kW	522 kW
BESS capacity	367 kWh	1721 kWh
Electrified berths	2-3-4	2–4
Hydrogen generator multi-stack fuel cell system maximum power	400 kW	300 kW
Hydrogen generator battery capacity	460 kWh	979 kWh
Berths covered by the hydrogen generator	1–5	1-3-5
Number of CMS	3	2
Number of mobile hydrogen generator	1	2
Substation costs (including distribution and the BESS)		
Total CAPEX	$1,280,332	$1,305,232
Annualized CAPEX	$100,156	$102,104
Annual OPEX	$143,416	$101,729

(*continued on next page*)

Table 4 (*continued*)

Variable	Proposed bilevel model	Central single layer model
Mobile hydrogen generator costs		
Total CAPEX	$629,250	$1,313,550
Annualized CAPEX	$49,224	$108,996
Annual OPEX	$9969	$86,795
Total annual profit	-$170,209	-$267,067

The benchmark comparison in Table 4 indicates that the simplified centralized formulation is 36% more expensive and systematically trades substation capacity for conservative asset oversizing, resulting in lower economic performance than the bilevel model. In particular, the centralized model selects a substantially smaller substation rating (522 kW vs. 891 kW) but compensates with markedly larger storage and mobile generation capacities and electrical distribution layout (BESS: 1721 kWh vs. 367 kWh; only 2 berths covered by the substation instead of one, two hydrogen generators vs. one), which increases total CAPEX and hydrogen-related OPEX. This behaviour is expected because the centralized benchmark does not include an explicit operational dispatch optimizer. Feasibility is enforced through conservative sizing inequalities to satisfy peak and autonomy requirements, which tends to inflate installed capacities and lifecycle costs.

Lower-level optimality analysis

The optimality of the lower-level linear dual-simplex algorithm was evaluated by comparing its results to a dynamic programming equivalent algorithm. Based on Bellman's principle of optimality, the dynamic programming method guarantees that any optimal dispatch trajectory contains optimal sub-trajectories, and therefore provides a robust reference for global optimality by recursively minimizing the cost-to-go over discretized states [47]. In this case, the state is the battery state-of-charge discretized with a step of 0.1, and the demand-charge search over the grid peak uses a precision step of 0.1. The reference population for the upper-level algorithm is $P_{max}^{Subst} = 1500\,kW, Q^{BESS} = 800\,kWh, N_s = 4,\ Q^{BHGen} = 700, l = \{\{2,3,4\},\{1,5\}\}$. Table 5 reports the computational performance, solution quality, and variation of the linear model compared to the dynamic programming model.

Table 5
Lower-level algorithm optimality analysis.

	Dynamic programming algorithm	Proposed linear programming algorithm	Relative difference
Algorithm running time	238.5 ms	89.1 ms	−62.6%
Optimal electrical cost of energy	$401.29	$402.60	+0.33%
Optimal electrical cost of power	$7099.50	$7059.10	+0.57%

Table 5 shows that the linear dual-simplex formulation yields dispatch costs that closely match the dynamic-programming reference, with differences below 1% for both the energy and demand-charge components. Because dynamic programming is optimal within the chosen discretization, this result supports the near-optimality of the proposed lower-level solver while confirming its superior computational efficiency. The remaining deviations are attributed to discretization effects and resolution differences between the two methods.

Port electrical pricing investigation

The subsection presents a tariff-sensitivity analysis comparing four electricity-pricing schemes for the port compared to the utility grid: the reference demand-charge tariff, a fixed per-kWh tariff, a time-of-use (TOU) tariff, and a day-ahead market-based tariff. For each pricing case, the bilevel model was used using identical input data and constraints. Only the reference demand-charge tariff has a price on power ($/kW). For the TOU tariff, the varying electricity cost was applied at each hour of the day, considering the season. For the day-ahead market-based tariff, a typical daily pattern was used as a reference for all days. The results are summarized in Table 6.

Table 6
Comparison analysis of different electricity pricing tariffs on the model in USD.

	Demand-charge tariff (Reference)	Fixed electrical cost tariff	TOU tariff	Day ahead tariff
Electrical pricing	¢11.60/kW ¢3.37/kWh	¢15/kWh	Peak: ¢15.23/kWh Mid-peak: ¢11.77/kWh Off-peak: ¢7.35/kWh	Between ~¢10/kWh and ~¢32/kWh
Tariff source	Hydro-Québec M tariff [48]	Average cost	Hydro One TOU winter and summer tariff [49]	Based on the day-ahead Ontario zonal price [50]
Design parameters				
Substation maximum budgeted power	891 kW	970 kW	969 kW	954 kW
BESS capacity	367 kWh	–	2 kW	32 kW
Electrified berths	2-3-4	2-3-4	2-3-4	1-2-3-4-5
Hydrogen generator multi-stack fuel cell system maximum power	400 kW	400 kW	400 kW	400 kW
Hydrogen generator battery capacity	460 kWh	460 kWh	460 kWh	460 kWh
Berths covered by the hydrogen generator	1–5	1–5	1–5	1–5

(*continued on next page*)

Table 6 (*continued*)

	Demand-charge tariff (Reference)	Fixed electrical cost tariff	TOU tariff	Day ahead tariff
Number of CMS	3	3	3	3
Number of mobile hydrogen generator	1	1	1	1
Substation costs (including distribution and the BESS)				
Total CAPEX	$1,280,332	$1,217,508	$1,217,708	$1,220,708
Annualized CAPEX	$100,156	$95,242	$95,257	$95,492
Annual OPEX	$143,416	$136,340	$98,830	$125,899
Mobile hydrogen generator costs				
Total CAPEX	$629,250	$629,250	$629,250	$629,250
Annualized CAPEX	$49,224	$49,224	$49,224	$49,224
Annual OPEX	$9969	$9969	$9969	$9969
Total annual profit	-$170,209	-$158,218	-$120,723	-$148,027

Under the reference demand-charge tariff, the model selects a moderate substation rating of 891 kW combined with a 367 kWh BESS, confirming that storage is economically justified when peak power charges are explicitly penalized. When the tariff structure does not include a demand component, the optimal BESS capacity is reduced to zero or near zero, and the substation rating increases to approximately 950–970 kW. This indicates that, in the present formulation, storage is primarily valued for peak shaving rather than for energy price-shifting.

The TOU tariff yields the best economic outcome among the tested cases, with an annual profit of –$120 k, mainly due to lower operational expenditures. However, the optimal storage capacity remains negligible, as the model does not explicitly reward inter-temporal energy price-shifting beyond simple cost minimization. Similarly, under the fixed and day-ahead tariffs, the absence of a binding peak-demand constraint or explicit power-capacity cost weakens the incentive to install storage. As a result, the BESS is not economically retained, and the optimization relies primarily on grid supply.

These results highlight a structural limitation of the current formulation. The model is particularly well suited to demand-charge environments, where peak power directly drives investment and operational decisions. In tariff regimes dominated by energy pricing, the peak power demand is neither constrained nor priced in a way that preserves the economic value of storage, leading to minimal BESS sizing. Further adaptations are therefore required to better represent the economic dynamics of TOU, fixed, and day-ahead tariff structures, especially if storage participation in energy markets or grid services is to be considered.

In addition, the present formulation does not investigate the case where the BESS could be dispatched outside ship-demand periods to sell electricity back to the grid or participate in ancillary services. Including such operational strategies would likely modify the optimal storage sizing under energy-based tariffs and should be examined in future developments of the model.

Complementary berth usage analysis

Regarding the dependence of optimal designs on berth-utilization assumptions, this section investigates different utilization scenarios. Table 7 reports the bilevel model outcomes under four additional berth-usage distributions, Scenarios 2–5, with the first scenario being the reference test case scenario. The scenarios are designed to span plausible utilization patterns ranging from uniform moderate use to highly concentrated demand and high overall activity. For each scenario, the model is re-solved using identical cost and tariff assumptions, and the resulting optimal infrastructure sizing, layout selection, and economic performance are compared to the reference test case.

- Scenario 1 (Reference, realistic scenario): berth 1–5 utilization = [3%, 25%, 22%, 15%, 1%]. The combined total utilization is 66%.
- Scenario 2 (uniform moderate utilization): berth 1–5 utilization = [13.2%, 13.2%, 13.2%, 13.2%, 13.2%]. The combined total utilization is 66%.
- Scenario 3 (highly concentrated at remote/low-network berths): berth 1–5 utilization = [31.5%, 1%, 1%, 1%, 31.5%]. The combined total utilization is 66%.
- Scenario 4 (high overall utilization): berth 1–5 utilization = [40%, 40%, 40%, 40%, 40%]. The combined total utilization is 200%.
- Scenario 5 (uniform low utilization): berth 1–5 utilization = [5%, 5%, 5%, 5%, 5%]. The combined total utilization is 25%.

Table 7
Comparison analysis of different berth utilization scenarios in USD.

	Scenario 1	Scenario 2	Scenario 3	Scenario 4	Scenario 5
Design parameters					
Substation maximum budgeted power	891 kW	1182 kW	534 kW	1182 kW	331 kW
BESS capacity	367 kWh	397 kWh	449 kW	397 kW	181 kW
Electrified berths	2-3-4	2-3-4-5	1–5	2-3-4-5	1
Hydrogen generator multi-stack fuel cell system maximum power	400 kW	400 kW	400 kW	400 kW	400 kW
Hydrogen generator battery capacity	460 kWh	460 kWh	648 kWh	460 kWh	648 kWh
Berths covered by the hydrogen generator	1–5	1	2-3-4	1	2-3-4-5
Number of CMS	3	3	2	4	1
Number of mobile hydrogen generator	1	1	1	1	2
Substation costs (including distribution and the BESS)					
Total CAPEX	$1,280,332	$1,509,832	$1,397,032	$1,697,332	$498,482
Annualized CAPEX	$100,156	$118,109	$109,285	$132,777	$38,995

(*continued on next page*)

Table 7 (*continued*)

	Scenario 1	Scenario 2	Scenario 3	Scenario 4	Scenario 5
Annual OPEX	$143,416	$175,011	$91,487	$225,814	$43,681
Mobile hydrogen generator costs					
Total CAPEX	$629,250	$629,250	$671,550	$629,250	$1,193,100
Annualized CAPEX	$49,224	$50,976	$52,533	$57,976	$100,458
Annual OPEX	$9969	$32,900	$9674	$99,697	$60,834
Total annual profit	-$170,209	-$252,132	-$151,286	-$134,875	-$196,530

Table 7 shows that berth-utilization patterns materially influence both the optimal topology (electrified-network extent versus mobile hydrogen coverage) and the resulting sizing of the substation and storage. When utilization is broadly distributed across berths and high, the model tends to favour a fully electrified network with larger grid-facing capacity and storage to manage peaks, whereas more concentrated or low-utilization patterns increase the attractiveness of mobile hydrogen generation for selected berths by avoiding fixed-network expansion. Across scenarios, the economic outcome remains strongly driven by the interaction between utilization and demand-charge exposure, highlighting why ports must provide scenario-based utilization forecasts when applying the model for planning. Finally, the high-utilization scenario, Scenario 4, has the overall best profit, indicating how optimizing utilization or targeting ports with high utilization rates benefits shore power.

Data availability

Data will be made available on request.

References

[1] J. Faber, et al., REDUCTION OF GHG EMISSIONS FROM SHIPS Fourth IMO GHG Study 2020 – Final report [Online]. Available: https://docs.imo.org, Jul. 2020.

[2] A.-R. Kim, J. Seo, Y.-J. Seo, Key barriers to adopting onshore power supply to reduce port air pollution: policy implications for the maritime industry in South Korea, Mar. Policy 157 (Nov. 2023) 105866, https://doi.org/10.1016/j.marpol.2023.105866.

[3] H. Daniel, J.P.F. Trovão, D. Williams, Shore power as a first step toward shipping decarbonization and related policy impact on a dry bulk cargo carrier, eTransportation 11 (2022) 100150 février, doi:EP.

[4] Ç. Iris, J.S.L. Lam, A review of energy efficiency in ports: operational strategies, technologies and energy management systems, Renew. Sust. Energ. Rev. 112 (Sep. 2019) 170–182, https://doi.org/10.1016/j.rser.2019.04.069.

[5] V. Semchukova, K. Topolski, Z. Abdin, Hydrogen technology for maritime applications: a review of challenges, opportunities, and lessons from the port authority of New York and New Jersey, Renew. Sust. Energ. Rev. 216 (Jul. 2025) 115641, https://doi.org/10.1016/j.rser.2025.115641.

[6] A. Sinha, P. Malo, K. Deb, A review on bilevel optimization: from classical to evolutionary approaches and applications, IEEE Trans. Evol. Comput. 22 (2) (Apr. 2018) 276–295, https://doi.org/10.1109/TEVC.2017.2712906.

[7] A. Innes, J. Monios, Identifying the unique challenges of installing cold ironing at small and medium ports – the case of Aberdeen, Transp. Res. Part Transp. Environ. 62 (Jul. 2018) 298–313, https://doi.org/10.1016/j.trd.2018.02.004.

[8] J.E. Gutierrez-Romero, J. Esteve-Pérez, B. Zamora, Implementing onshore power supply from renewable energy sources for requirements of ships at Berth, Appl. Energy 255 (Dec. 2019) 113883, https://doi.org/10.1016/j.apenergy.2019.113883.

[9] G. Caprara, L. Martirano, M. Kermani, D. de Mesquita e Sousa, R. Barilli, V. Armas, Cold ironing and battery energy storage system in the port of Civitavecchia, in: 2022 IEEE International Conference on Environment and Electrical Engineering and 2022 IEEE Industrial and Commercial Power Systems Europe (EEEIC/I&CPS Europe), Jun. 2022, pp. 1–6, https://doi.org/10.1109/EEEIC/ICPSEurope54979.2022.9854593.

[10] Ç. Iris, J.S.L. Lam, Optimal energy management and operations planning in seaports with smart grid while harnessing renewable energy under uncertainty, Omega 103 (Sep. 2021) 102445, https://doi.org/10.1016/j.omega.2021.102445.

[11] R. Tang, Z. Wu, X. Li, Optimal power flow dispatching of maritime hybrid energy system using model predictive control, Energy Procedia 158 (Feb. 2019) 6183–6188, https://doi.org/10.1016/j.egypro.2019.01.490.

[12] D. Xia, J. He, F. Chi, Z. Dou, Z. Yang, C. Liu, Shore power optimal scheduling based on gridding of hybrid energy supply system, Sustainability 14 (23) (Jan. 2022) 23, https://doi.org/10.3390/su142316250.

[13] J. Song, Q. Shan, T. Zou, J. Hu, F. Teng, Distributed energy management for zero-carbon port microgrid, Int. Trans. Electr. Energy Syst. Aug. 2022 (2022) e2752802, https://doi.org/10.1155/2022/2752802.

[14] F. Conte, F. D'Agostino, D. Kaza, S. Massucco, G. Natrella, F. Silvestro, Optimal management of a smart port with shore-connection and hydrogen supplying by stochastic model predictive control, in: 2022 IEEE Power & Energy Society General Meeting (PESGM), Jul. 2022, pp. 1–5, https://doi.org/10.1109/PESGM48719.2022.9916817.

[15] J. Wang, F. Teng, T. Yang, Q. Shan, Distributed energy management for port microgrid with we-energy, in: 2022 34th Chinese Control and Decision Conference (CCDC), Aug. 2022, pp. 1077–1081, https://doi.org/10.1109/CCDC55256.2022.10034015.

[16] Q. Zhang, Q. Shan, T. Li, Large port energy management based on distributed optimization, in: 2020 7th International Conference on Information, Cybernetics, and Computational Social Systems (ICCSS), Nov. 2020, pp. 108–113, https://doi.org/10.1109/ICCSS52145.2020.9336919.

[17] F.D. Kanellos, E.-S.M. Volanis, N.D. Hatziargyriou, Power management method for large ports with multi-agent systems, IEEE Trans. Smart Grid 10 (2) (Mar. 2019) 1259–1268, https://doi.org/10.1109/TSG.2017.2762001.

[18] N.B. Ahamad, M. Othman, J.C. Vasquez, J.M. Guerrero, C.-L. Su, Optimal sizing and performance evaluation of a renewable energy based microgrid in future seaports, in: 2018 IEEE International Conference on Industrial Technology (ICIT), Feb. 2018, pp. 1043–1048, https://doi.org/10.1109/ICIT.2018.8352322.

[19] A. Molavi, J. Shi, Y. Wu, G.J. Lim, Enabling smart ports through the integration of microgrids: a two-stage stochastic programming approach, Appl. Energy 258 (Jan. 2020) 114022, https://doi.org/10.1016/j.apenergy.2019.114022.

[20] W. Wang, Y. Peng, X. Li, Q. Qi, P. Feng, Y. Zhang, A two-stage framework for the optimal design of a hybrid renewable energy system for port application, Ocean Eng. 191 (Nov. 2019) 106555, https://doi.org/10.1016/j.oceaneng.2019.106555.

[21] S. Haghifam, K. Zare, M. Dadashi, Bi-level operational planning of microgrids with considering demand response technology and contingency analysis, Transm. Distrib. IET Gener. 13 (13) (2019) 2721–2730, https://doi.org/10.1049/iet-gtd.2018.6516.

[22] A. Letafat, et al., Simultaneous energy management and optimal components sizing of a zero-emission ferry boat, J. Energy Storage 28 (Apr. 2020) 101215, https://doi.org/10.1016/j.est.2020.101215.

[23] M. Hajiaghaei-Keshteli, A.M. Fathollahi-Fard, A set of efficient heuristics and metaheuristics to solve a two-stage stochastic bi-level decision-making model for the distribution network problem, Comput. Ind. Eng. 123 (Sep. 2018) 378–395, https://doi.org/10.1016/j.cie.2018.07.009.

[24] M.J. Alves, C.H. Antunes, I. Soares, Optimizing prices and periods in time-of-use electricity tariff design using bilevel programming, in: L. Paquete, C. Zarges (Eds.), Evolutionary Computation in Combinatorial Optimization, Springer International Publishing, Cham, 2020, pp. 1–17, https://doi.org/10.1007/978-3-030-43680-3_1.

[25] S. Arif, T. Aziz, Study of transient stability with battery energy storage systems in renewable integrated islanded microgrid, in: 2017 IEEE International WIE Conference on Electrical and Computer Engineering (WIECON-ECE), Dec. 2017, pp. 266–269, https://doi.org/10.1109/WIECON-ECE.2017.8468905.

[26] V.K. Chauhan, M. Sahu, J. Bhattacharya, Thermal characterization of 18650 lithium iron phosphate cell for wide ranges of temperature and discharge rate to identify most efficient operating window, J. Energy Storage 119 (May 2025) 116274, https://doi.org/10.1016/j.est.2025.116274.

[27] B. Xu, A. Oudalov, A. Ulbig, G. Andersson, D.S. Kirschen, Modeling of lithium-ion battery degradation for cell life assessment, IEEE Trans. Smart Grid 9 (2) (Mar. 2018) 1131–1140, https://doi.org/10.1109/TSG.2016.2578950.

[28] A. Barré, B. Deguilhem, S. Grolleau, M. Gérard, F. Suard, D. Riu, A review on lithium-ion battery ageing mechanisms and estimations for automotive applications, J. Power Sources 241 (Nov. 2013) 680–689, https://doi.org/10.1016/j.jpowsour.2013.05.040.

[29] R. Ghaderi, M. Kandidayeni, M. Soleymani, L. Boulon, J.P.F. Trovão, Online health-conscious energy management strategy for a hybrid multi-stack fuel cell vehicle based on game theory, IEEE Trans. Veh. Technol. 71 (6) (Jun. 2022) 5704–5714, https://doi.org/10.1109/TVT.2022.3167319.

[30] C. Houchins, J. Brian D., 2020 DOE Hydrogen and Fuel Cells Program Review Hydrogen Storage Cost Analysis, Strategic Analysis Inc., May 2020 [Online]. Available: https://www.hydrogen.energy.gov/docs/hydrogenprogramlibraries/pdfs/st100_houchins_2020_o.pdf?Status=Master.

[31] A.J. Headley, S. Schoenung, "CHAPTER 11 HYDROGEN ENERGY STORAGE," in U. S. DOE Energy Storage Handbook, Ongoing book [Online], 2013. Available: https://www.sandia.gov/ess/publications/doe-oe-resources/eshb.

[32] J.W. Pratt, S.H. Chan, Maritime Fuel Cell Generator Project, Sandia National Laboratories, Albuquerque, New Mexico 87185 and Livermore, California 94550, May 2017. SAND2017-5751.
[33] H. Chen, P. Pei, M. Song, Lifetime prediction and the economic lifetime of proton exchange membrane fuel cells, Appl. Energy 142 (Mar. 2015) 154–163, https://doi.org/10.1016/j.apenergy.2014.12.062.
[34] Cooperative optimization of shore power allocation and berth allocation: a balance between cost and environmental benefit, J. Clean. Prod. 279 (Jan. 2021) 123816, https://doi.org/10.1016/j.jclepro.2020.123816.
[35] C.H. Antunes, M.J. Alves, J. Clímaco, Multiobjective linear and integer programming, in: EURO Advanced Tutorials on Operational Research, Springer International Publishing, 2016, https://doi.org/10.1007/978-3-319-28746-1.
[36] N. Ploskas, N. Samaras, Revised dual simplex algorithm, in: N. Ploskas, N. Samaras (Eds.), Linear Programming Using MATLAB®, Springer International Publishing, Cham, 2017, pp. 383–435, https://doi.org/10.1007/978-3-319-65919-0_9.
[37] H. Daniel, J.P.F. Trovão, D. Williams, L. Boulon, Unlocking shore power in St. Lawrence and Great Lakes for cargo ships, Transp. Res. Part Transp. Environ. 131 (Jun. 2024) 104230, https://doi.org/10.1016/j.trd.2024.104230.
[38] K. Mongird, V. Viswanathan, J. Alam, C. Vartanian, V. Sprenkle, R. Baxter, 2020 Grid Energy Storage Technology Cost and Performance Assessment, US Department of Energy, DOE/PA-0204, Dec. 2020 [Online]. Available: https://www.pnnl.gov/sites/default/files/media/file/Final%20-%20ESGC%20Cost%20Performance%20Report%2012-11-2020.pdf.
[39] A. Cichy, B. Sakowicz, M. Kaminski, Economic optimization of an underground power cable installation, IEEE Trans. Power Deliv. 33 (3) (Jul. 2017) 1124–1133, https://doi.org/10.1109/TPWRD.2017.2728702.
[40] IMAR, L'électrification des quais au Québec [Online]. Available: https://tmq.ca/wp-content/uploads/2022/05/Electrification-des-quais-au-Quebec-MeRLIN-IMAR.pdf, 2022.
[41] Hydro-Quebec, Tarifs d'électricité d'Hydro-Québec dans ses activités de distribution d'électricité, en vigueur le 1er avril 2025, in: Hydro-Québec, Bibliothèque et Archives nationales du Québec, 2025. Accessed: Mar. 24, 2026. [Online]. Available: https://www.hydroquebec.com/documents-donnees/publications-officielles/tarifs-conditions-service.html.
[42] K. Gregory, W. Gibbons, J. Fornaciari, Heavy-Duty Fuel Cell System Cost – 2022, Department of Energy, United States of America, DOE Hydrogen Program Record, May 2023 [Online]. Available: https://www.hydrogen.energy.gov/docs/hydrogenprogramlibraries/pdfs/23002-hd-fuel-cell-system-cost-2022.pdf?Status=Master.
[43] B. Sharpe, H. Basma, A Meta-study of Purchase Costs for Zero-emission Trucks - International Council on Clean Transportation, ICCT, Feb. 2022. Accessed: Dec. 06, 2024. [Online]. Available: https://theicct.org/publication/purchase-cost-ze-trucks-feb22/.
[44] M.G. Rasul, M.A. Hazrat, M.A. Sattar, M.I. Jahirul, M.J. Shearer, The future of hydrogen: challenges on production, storage and applications, Energy Convers. Manag. 272 (Nov. 2022) 116326, https://doi.org/10.1016/j.enconman.2022.116326.
[45] US EPA, Eastern Research Group, Inc, and Energy & Environmental Research Associates, LLC, Shore Power Technology Assessment at U.S. Ports, U.S. Environmental Protection Agency, Dec. 2022. Reports and Assessments EPA-420-R-22-037. [Online]. Available: https://www.epa.gov/ports-initiative/shore-power-technology-assessment-us-ports.
[46] H. Daniel, J.P.F. Trovão, D. Williams, L. Boulon, A journey into electrical standardization of shore power connections for bulk carriers: development of a bulk carrier and general cargo ship standard for shore power connections in port, IEEE Electrif. Mag. 12 (4) (Dec. 2024) 84–94, https://doi.org/10.1109/MELE.2024.3473334.
[47] R. Bellman, The theory of dynamic programming, Bull. Am. Math. Soc. 60 (6) (1954) 503–515, https://doi.org/10.1090/S0002-9904-1954-09848-8.
[48] Hydro-Québec, Tarifs d'électricité en vigueur le 1er avril 2025, Québec. [Online]. Available: https://www.hydroquebec.com/data/documents-donnees/pdf/tarifs-electricite.pdf?v=20260109, 2025.
[49] Hydro One, Hydro One - TOU tariff, 2026 [Online]. Available: https://www.hydroone.com:443/rates-and-billing/rates-and-charges/electricity-pricing-and-costs. Accessed: Feb. 11, 2026.
[50] ISEO, ISEO - Data Directory, 2026 [Online]. Available: https://www.ieso.ca/Power-Data/Data-Directory. Accessed: Feb. 11, 2026.